



HIDES spectroscopy of bright detached eclipsing binaries from the *Kepler* field – III. Spectral analysis, updated parameters and new systems

K. G. Hełminiak^{1,2} M. Konacki,¹ H. Maehara,² E. Kambe,^{2,3} N. Ukita,^{2,4}
M. Ratajczak,^{5,6} A. Pigulski⁶ and S. K. Kozłowski¹

¹ Nicolaus Copernicus Astronomical Center, Polish Academy of Sciences, ul. Rabiańska 8, 87-100 Toruń, Poland

² Okayama Astrophysical Observatory, National Astronomical Observatory of Japan, 3037-5 Honjo, Kamogata, Asakuchi, Okayama 719-0232, Japan

³ Subaru Telescope, National Astronomical Observatory of Japan, 650 North Aohoku Place, Hilo, HI 96720, USA

⁴ The Graduate University for Advanced Studies, 2-21-1 Osawa, Mitaka, Tokyo 181-8588, Japan

⁵ Warsaw University Astronomical Observatory, Al. Ujazdowskie 4, 00-478 Warszawa, Poland

⁶ Instytut Astronomiczny, Uniwersytet Wrocławski, ul. Kopernika 11, 51-622 Wrocław, Poland

Accepted 2018 December 21. Received 2018 December 21; in original form 2018 October 27

ABSTRACT

We present the latest results of our spectroscopic observations and refined modelling of a sample of detached eclipsing binaries, selected from the *Kepler* Eclipsing Binary Catalog, that are also double-lined spectroscopic binaries (SB2s). New high-resolution spectra obtained with the HIgh-Dispersion Echelle Spectrograph (HIDES), attached to the 1.88-m telescope of the Okayama Astrophysical Observatory, have supplemented the previous observations. This has allowed us to improve the physical parameters of some systems, and to characterize three previously omitted objects. All the obtained radial velocities were combined with *Kepler* photometry, in order to derive a full set of orbital and physical parameters. Ten out of eleven SB2s have their component spectra tomographically disentangled, and spectral analysis was performed with ISPEC, in order to derive the effective temperatures of components and the metallicities of the systems. By comparing our results with theoretical models, we assess the age and evolutionary status of the studied objects. We find a good match to all systems but one. We have derived distances from the parameters determined in this way, and we compare them with those from the *Gaia* Data Release 2. For systems previously studied by other authors, our new results lead to better consistency between observations and models.

Key words: binaries: eclipsing – binaries: spectroscopic – stars: evolution – stars: fundamental parameters – stars: late-type.

1 INTRODUCTION

A great source of absolute fundamental parameters of stars are detached eclipsing binaries (DEBs) that are also double-lined spectroscopic binaries (SB2s). For decades, these have been used in stellar astrophysics (but not only) for many purposes, such as for testing models of stellar structure and evolution or for creating empirical relations between various stellar parameters, later used as calibrations for studies of single stars, such as exoplanet hosts. To be useful, the resulting quantities must be known with sufficient precision (believed to be $\sim 2\text{--}3$ per cent in masses and radii; Lattner & Valls-Gabaud 2002; Torres, Andersen & Giménez 2010) and the set of presented parameters must be as complete as possible, and should include individual effective temperatures of components and, preferably, information about the chemical composition, such

as metallicity and/or abundances, of the most important elements (e.g. He, Fe, α -elements). The precision in absolute physical parameters can be reached with high-quality radial velocities (RVs) and time-series photometry. The former can be calculated from high-resolution spectra obtained with spectrographs of sufficient stability. The most precise photometry comes from space-based observatories, such as *CoRoT*, *Kepler* and the *Transiting Exoplanet Survey Satellite* (*TESS*). The atmospheric parameters usually come from the analysis of stellar spectra, provided that the individual spectra are properly separated from each other.

For all these reasons, we were motivated to pursue our programme of high-resolution spectroscopic monitoring of a sample of bright DEBs from the original *Kepler* field. We aimed for as precise and complete a characterization of the observed system as possible, with the aid of the unprecedented precision of the *Kepler* light curves (LCs). The programme was conducted between 2014 July and 2017 November using the 1.88-m telescope of the

* E-mail: xy siek@ncac.torun.pl

Okayama Astrophysical Observatory (OAO), equipped with the HIgh-Dispersion Echelle Spectrograph (HIDES; Izumiura 1999). In this paper, we present new spectroscopic observations, including three new objects, updated orbital solutions and, for the first time in this project, spectroscopic analysis of tomographically disentangled spectra, from which we mainly obtain the effective temperatures and metallicities that are later used for the determination of ages. The paper is organized as follows. In Section 2, we present our final sample of eclipsing SB2s. In Section 3, we present the methodology, with the focus put on new data and spectroscopic analysis. In Section 4, we present the results, including an extended set of parameters, a comparison with literature data and theoretical models that utilizes the newly obtained atmospheric parameters and a new hypothesis regarding the tertiary companion to an eclipsing SB2. In Section 5, we give our conclusions about our findings. Finally, in Appendix A, we present updated information about one SB1 system from our project that was also re-observed recently.

2 THE FINAL SAMPLE OF TARGETS

In our spectroscopic programme dedicated to bright objects from the *Kepler* Eclipsing Binary Catalog (KEBC; Prša et al. 2011; Slawson et al. 2011; Kirk et al. 2016),¹ we observed a total of 22 systems with various characteristics: from blends with background stars, through single- and double-lined spectroscopic binaries, to multiples containing as many as five components. The basic target selection criteria were as follows.

(i) *Kepler* magnitude $kmag < 11.5$, in order to have the targets within the brightness range of the telescope. This criterion was initially $kmag < 11.0$, but it changed in 2016, when several systems fainter than $kmag = 11$ were included.

(ii) Morphology parameter (Matijević et al. 2012) $morph < 0.6$, in order to exclude contact and semidetached configurations.

(iii) Effective temperature $T_{\text{eff}} < 6700$ K, in order to have only late-type systems, with many spectral features. We queried the temperatures from the *Kepler* Input Catalog (KIC; Kepler Mission Team 2009), although some of our objects turned out to be hotter.

Out of the 22 systems observed, to date we have published data and analysed 19 of them: nine single-lined binaries were studied in Helminiak et al. (2016, hereafter Paper I), eight double- and triple-lined systems were studied in Helminiak et al. (2017a, hereafter Paper II), the double-giant system KIC 9246715 was presented in Helminiak et al. (2015a, hereafter K924) and a multi-eclipsing quintuple KIC 4150611 was presented in Paper II. In this paper, we focus on 11 systems, presenting new data for four objects, and three entirely new pairs, not yet studied. One of the previously described targets with new observations – KIC 10191056 – is a triple-lined system that includes an eclipsing SB2 component (KIC 10191056 A). This system is the only one in this work for which we did not perform spectral disentangling and analysis. Spectral analysis of another triple-lined system – KIC 6525196 – is a subject of another dedicated paper (Alicavus et al., in preparation). Flux of the multiple KIC 4150611 is dominated by a hybrid δ Scuti/ γ Doradus (δ Sct/ γ Dor) pulsator, which itself was also studied spectroscopically, and its metallicity and age have been estimated (Niemczura et al. 2015; Paper II). Here we also introduce three new SB2s, for which we apply the same working approach as for the rest of the sample.

Below, we briefly describe the new objects. Similar descriptions of other targets can be found in Paper II and K924. Unless stated otherwise, this work is the first detailed study for a particular object.

KIC 3439031 = KOI 4980, TYC 3134-978-1. This system shows nearly equal, deep (~ 50 per cent) eclipses, suggesting it is composed of two very similar stars. Except for brightness and position measurements, no data important for this study are available in the literature.

KIC 4851217 = KOI 6460, HD 225524, HAT 199-10019, ASAS J194320+3957.1. The LC of this system shows strong ellipsoidal variations and, despite the short orbital period (2.47 d), the separation of two minima in phase is different from 0.5, meaning a non-zero eccentricity. It has been identified as an eclipsing variable by the HATNET Variability Survey (Hartman et al. 2004), and also listed later in the catalogue of variable stars in the *Kepler* field of view of the All-Sky Automated Survey (ASAS-K; Pigulski et al. 2009). Its eclipse timing variations (ETVs) were studied by Gies et al. (2012, 2015) and Conroy et al. (2014), and a long-term, parabolic trend in timing of both primary and secondary minima was noted. Furthermore, Gies et al. (2012) reported pulsations in the LC, which were later confirmed to be of a δ Sct type (Fedurco, private communication). Finally, Matson et al. (2017) collected a number of medium-resolution spectra ($R \simeq 4000$ –6200), and derived a preliminary set of orbital and physical parameters, such as $M_1 = 1.43(5)$ and $M_2 = 1.55(5) M_{\odot}$, which we can compare with our results.

KIC 10583181 = KOI 7344, T-Lyr1-01013, TYC 3544-2565-1. This system was known as a DEB before the launch of *Kepler*. It was identified by the Trans-Atlantic Exoplanet Survey (TrES; Alonso et al. 2004). The *Kepler* LC shows that the secondary eclipse is flat (occultation). By analysing the TrES data only, Devor et al. (2008) estimated the masses of both components: 1.749(19) and 1.049(15) M_{\odot} for the primary and secondary, respectively. Our spectroscopy allows us to revise these values. Later, Borkovits et al. (2016) detected strong ETVs with the period of ~ 3.2 yr, and derived parameters of the outer orbit. Their solution predicted that the modulation of the systemic velocity γ of the eclipsing pair will be about 13 km s^{-1} (peak-to-peak), large enough to be detectable with our spectroscopy.

3 DATA AND ANALYSIS

We follow the same methodology as in Papers I, II and K924. They present the observations, sources of publicly available data, RV calculations, and approach to RV and LC fitting. Here we only describe these briefly, and we focus more on things that were not previously presented.

3.1 New spectroscopy and RVs

As in previous works, the HIDES instrument was fed through a circular fibre, for which the light is collected via a circular aperture of projected on-sky diameter of 2.7 arcsec, drilled in a flat mirror that is used for guiding (Kambe et al. 2013). An image slicer is used in order to reach both high resolution ($R \sim 50\,000$) and good efficiency of the system. Spectra extraction was performed using IRAF,² with

¹<http://keplerebs.villanova.edu/>

procedures dedicated to HIDES. The wavelength solution was based on ThAr exposures taken every 1–2 h, which allows for stability of the order of $\sim 40 \text{ m s}^{-1}$. The resulting spectra span from 4360 to 7535 Å.

The newly presented HIDES observations were carried out during several runs between 2016 May and 2017 November, with the new observations of objects previously described taking place after 2016 October. During that time, a new queue scheduling mode was introduced at the OAO-1.88, and the final observations were carried out in this way, instead of visitor mode.

As in Paper I, we also made use of the data collected by the Apache Point Observatory Galactic Evolution Experiment (APOGEE; Allende Prieto et al. 2008; Majewski et al. 2017). We have extracted six individual visit spectra³ of KIC 4851217, but this time we calculated the RVs ourselves, instead of using the values given by the survey, as in Paper I. Unfortunately, only three of them were recorded when the velocity difference between the components was large enough to be securely measured. Additionally, single archival spectra of KIC 4851217 and KIC 10191056 have been found on their ExoFOP-Kepler websites.⁴ These spectra ($R \sim 40\,000$) were taken on 2014 July 14 (KIC 10191056) and 2015 June 11 (KIC 4851217) with the Tillinghast Reflector Echelle Spectrograph (TRES), attached to the 1.5-m Tillinghast telescope of the Fred Lawrence Whipple Observatory (FLWO) in Arizona, USA. Two more targets have their TRES spectra available through ExoFOP (i.e. KIC 3439031 and KIC 8552540) but these observations do not influence the final solution significantly, and the measured RVs agree with models.

Finally, the RVs of several of our targets have been reported and analysed by Matson et al. (2017). Apart from the aforementioned KIC 4851217, these are KIC 8552540 and KIC 10191056. For the latter two objects, the agreement between Paper II and Matson et al. (2017) is, generally, very good. We do not include their RVs in our analysis, as the spectra were taken with lower resolution, and their inclusion does not change our results significantly.

RV measurements were done with our own implementation of the TODCOR technique (Zucker & Mazeh 1994), which finds velocities of two stars v_1 and v_2 simultaneously. As templates for the HIDES and TRES data, we used synthetic spectra computed with ATLAS9 and ATLAS12 codes (Kurucz 1992), which do not reach wavelengths longer than 6500 Å. For the APOGEE observations, we used synthetic spectra from the library of Coelho et al. (2005), which cover both optical and infrared regions (3800–18 000 Å), but have lower resolution than the ones from ATLAS9/12. Single measurement errors were calculated with a bootstrap approach (Helminiak et al. 2012), and used for weighting the measurements during the orbital fit, as they are sensitive to the signal-to-noise ratio (S/N) of the spectra and rotational broadening of the lines. All (previous and new) individual RV measurements are presented in Table B1 in the Appendix.

3.2 Kepler photometry

The RVs were supplemented by the long- and short-cadence *Kepler* photometry, which is available for download from the KEBC. We used the de-trended relative flux measurements f_{dtr} , that were later transformed into magnitude difference $\Delta m = -2.5 \log(f_{\text{dtr}})$, and finally the catalogue value of $kmag$ was added. From the systems

presented here, only KIC 9246715 and KIC 10987439 do not have short-cadence data available.

Even though our new systems have time-series photometry available from other sources, such as the TrES, we only work on the *Kepler* data. A comparison of solutions based on *Kepler* observations with those based on TrES or ASAS data, has been discussed in Paper II.

3.3 Orbital solutions

The orbital solutions were found using our own procedure called v2FIT (Konacki et al. 2010). We used it mainly to fit a double-Keplerian orbit to a set of RV measurements of two components, utilizing the Levenberg–Marquardt minimization scheme. The fitted parameters are the orbital period P , zero-phase T_p ,⁵ systemic velocity γ , velocity semi-amplitudes $K_{1,2}$, eccentricity e and periastron longitude ω . Depending on the case, we also included such effects as the difference between systemic velocities of two components, $\gamma_2 - \gamma_1$, linear and quadratic trends, or the periodic modulation of γ caused by a circumbinary body on an outer orbit, parametrized analogously by orbital parameters P_3 , T_3 , K_3 , e_3 and ω_3 . In such a case, γ is defined in the code as the systemic velocity of the whole triple. Whenever applicable, we simplified our fit by keeping the orbital period on the value given in the KEBC. Whenever $\gamma_2 - \gamma_1$ or e were found to be not significantly different from zero, the fit was repeated with those parameters fixed to 0. For KIC 4851217, we also searched for the difference between the zero-points of HIDES and APOGEE. This was not done for HIDES versus TRES zero-points, because only one TRES spectrum per target is available.

Systematics that come from fixing a certain parameter in the fit are assessed by a Monte Carlo (MC) procedure, and other possible systematics (e.g. coming from poor sampling, low number of measurements, pulsations, etc.) by a bootstrap analysis. All the uncertainties of orbital parameters given in this work already include the systematics.

Moreover, in order to obtain reliable formal parameter errors of the fit, and so that the final reduced χ^2 is close to 1, we modified the RV measurement errors either by adding a systematic term (jitter) in quadrature, or by multiplying by a certain factor. Adding the jitter works better for active stars, when the RV scatter is caused by spots, and is compensated with the additional term. However, as v2FIT weights the measurements on the basis of their own errors, which are sensitive to S/N and rotational velocity, we mainly used the second option, in which the weights are preserved.

3.4 Light-curve solutions

The *Kepler* LCs were fitted with the version 28 (v28) of the code JKTEBOP (Southworth, Maxted & Smalley 2004a; Southworth et al. 2004b), which is based on the EBOP program (Popper & Etzel 1981).

The short-cadence data, as a result of their denser time sampling, can include information that is missing in the long cadence (e.g. better represent short time-scale brightness variations, such as egress and ingress of some eclipses). We have therefore fitted both kinds of *Kepler* photometry, taking into account availability of the short-cadence data, and we have compared the output.

³<http://dr12.sdss3.org/advancedIRSearch>

⁴<https://exofop.ipac.caltech.edu/>

⁵Defined in this code as the moment of passing the pericentre for eccentric orbits or quadrature for circular.

Table 1. KEBC information about the targets from this work.

KIC	KOI	Other name	RA (deg)	Dec. (deg)	P (d) ^a	T_0 (BJD 245 0000) ^a	T_{eff}	$kmag$	d (pc) ^b	Stat. ^c
3439031	4980	TYC 3134-978-1	290.1327	38.5137	5.9520263	4954.068169	6337	11.287	486(6)	N
4851217	6460	HD 225524	295.8340	39.9523	2.4702800	4953.900507	6694	11.108	1195(53)	N
7821010	2938	TYC 3146-1340-1	291.3199	43.5955	24.238243	4969.615845	6298	10.816	360(5)	RL
8552540	7054	V2277 Cyg	288.8904	44.6170	1.0619343	4954.105667	5749	10.292	231(1)	–
9246715	7601	HD 190585	300.9514	45.6041	171.2776968	5170.514777	4699	9.266	616(11)	R
9641031	7211	FL Lyr	288.0203	46.3241	2.178154	4954.132713	5867	9.177	135.0(5)	RL
10031808	7278	HD 188872	298.7976	46.9302	8.589644	4956.430326	N/A ^d	9.557	474(6)	–
10191056 A	5774	BD+47 2717 A	283.8663	47.2283	2.4274949	4955.031469	6588	10.811	613(8)	RL
10583181	7344	T-Lyr-01013	283.7665	47.8190	2.6963227	4955.210895	6231	11.009	445(5)	N
10987439	7396	TYC 3561-922-1	296.8259	48.4434	10.6745992	4971.883920	6182	10.810	374(4)	–
11922782	7495	T-Cyg-00246	296.0074	50.2326	3.512934	4956.247158	5581	10.460	236(2)	–

^aFor the eclipsing binary, where T_0 is the primary eclipse mid-time.

^bFrom *Gaia* DR2 parallaxes (Prusti et al. 2016; Brown et al. 2018).

^cStatus of the system: ‘N’ = new, not described previously; ‘R’ = updated RV solution, new spectra presented in this work;

‘L’ = refined LC analysis; ‘–’ no new data, same solution as in previous papers, only ISPEC analysis added.

^dNo temperature given in the KEBC.

For long-cadence data, the errors were estimated with a residual-shift (RS) method (Southworth et al. 2011), run on data from each quarter separately, as described in Paper I. This was done in order to properly account for strong systematic effects of different time-scales (short-term pulsations or long-term evolution of spots). For short-cadence data, the same approach would take months of computer time, so instead of the RS method, we used the available MC option, also run on each quarter separately. In both cases, to obtain the final uncertainties, we added in quadrature the formal error of a weighted average of all available quarters, and the root mean square (rms) of the results from each quarter or set (Paper I).

Starting values of eccentricity e and periastron longitude ω , as well as mass ratio q (here held fixed), were taken from V2FIT runs. We fitted for the period P , the mid-time of the primary (deeper) minimum T_0 , the sum of the fractional radii $r_1 + r_2$ (where $r = R/a$), their ratio k , inclination i , surface brightness ratio J , maximum brightness S , as well as for e and ω (their final values are from the JKTEBOP runs, unless stated otherwise). Third light contribution I_3/I_{tot} , which can be significant in *Kepler* data, was also initially fitted for, but when it was found not significantly different from zero, or even negative, the fit was repeated with fixed $I_3/I_{\text{tot}} = 0$. The gravity darkening coefficients were always kept fixed at the values appropriate for stars with convective envelopes ($g = 0.32$). We did not fit for limb darkening (LD) coefficients, but we found them iteratively, as described in Paper II, and perturbed them in the RS or MC stage.

The final values of P and T_0 were derived from the complete long-cadence curves. However, because various systems show different LC characteristics (e.g. width of eclipses, ellipsoidal variations, pulsations, evolving spots, flares, timing variations, etc.), each binary has been treated individually. In the subsections describing results obtained for each target, we explicitly state if the adopted results come from short- or long-cadence LCs, if they are from fit to a complete curve, or if they are the weighted average from single-quarter curves, and which approach (RS or MC combined with rms) has been used to obtain uncertainties.

3.5 Tomographic spectra disentangling

In order to obtain separate spectra for each component, we performed tomographic disentangling (TD) of composite spectra

of 10 systems. This was done when at least eight good-quality observations were available, and only two sets of lines were clearly seen. For this reason, we omitted the triple-lined KIC 10191056, but included double-lined KIC 10583181, where significant third light was noted in the *Kepler* LC (Section 4).

We used the method described in Konacki et al. (2010), which is based on the tomographic approach proposed by Bagnuolo & Gies (1991). It utilizes prior RV measurements, which were made with TODCOR. The algorithm works on each echelle order separately, and is fragile to low-signal data. For this reason, the edges of each order were first trimmed, not every order was included or produced a satisfactory solution, and, in particular, we only used the orders from the ‘green’ chip of the HIDES detector.⁶ Therefore, the wavelength range of the final spectra varies from target to target. In a low number of cases, a given low-S/N spectrum was not used for TD, but still gave reasonably precise RV measurements. Before the TD, each order has been continuum-normalized. In the final steps, we merged the orders into single, long, one-dimensional spectra. In Table 2, we show for each star how many input spectra were used, what was the final wavelength range (including gaps), and what were the S/Ns of disentangled primary and secondary spectra. As the primary is defined by the LC, it is not always the brighter component.

We should note that two HIDES orders (96 and 97) containing the sodium D lines (around 5890 Å) did, formally, give a tomographic solution. However, the contamination from the interstellar Na introduced a third set of strong lines. Therefore, pieces of final spectra around the D lines were not recovered correctly and were not used in further analysis.

Before further analysis, the resulting TD spectra needed to be renormalized, in order to obtain the true intensities of the spectral lines. This can be done with the aid of additional information about the ratio of fluxes at a given wavelength (here, echelle order), which can be taken from TODCOR. The value of flux ratio α that maximizes the height of the cross-correlation can be calculated with a relatively simple analytical relation (equation A4 in Zucker & Mazeh 1994). The usage of TODCOR flux ratios has been shown to give proper results in, for example, Helminiak et al. (2015b) or Bright & Torres (2017).

⁶http://www.oao.nao.ac.jp/~hides/wiki/index.php?Mosaic_CCD_en

Table 2. Summary of TD information. Number of input spectra (N sp.), final wavelength range and S/Ns are given.

KIC	N sp.	Wavelength ranges (Å)	S/N ₁	S/N ₂
3439031	8	5030.555–6222.286	70	69
4851217	8	5030.316–6221.982	47	115
7821010	15	5265.545–6222.346	129	94
8552540	8	5030.468–6222.174	136	37
9246715	17	5030.582–5204.669; 5216.799–5400.960; 5417.327–5901.768; 5930.232–6222.319	123	117
9641031	14	5030.575–5400.956; 5417.321–6155.450	272	64
10031808	16	5030.582–5400.958; 5417.326–5841.582; 5930.227–6222.319	136	170
10583181	9	5030.323–6221.987	146	14
10987439	10	5469.778–5841.463; 5868.371–6222.195	20	134
11922782	10	5030.582–5204.667; 5216.978–6222.319	149	22

3.6 Spectroscopic analysis

The main motivation for this work was to complete the set of stellar parameters of the studied DEBs with effective temperatures and metallicities, which are necessary for further determination of the age and evolutionary status. For this, we used the v2018.06.08 version of the freely distributed code ISPEC (Blanco-Cuaresma et al. 2014) and our TD spectra. Each spectrum was first corrected for a residual RV shift, introduced in the TD stage (typically 0.3–0.5 km s $^{-1}$), and resampled with the wavelength step of 0.05 Å. The TD output is severely oversampled, so this step allowed us to reduce the number of data points in each spectrum, making the analysis about 10 times faster, while keeping the original HIDES resolution ($R \sim 50\,000$). To ensure the uncertainties given by ISPEC are trustworthy, we used the program to calculate reliable flux errors, based on the measured S/N of the spectra. With these errors, the reduced χ^2 of the fit was typically close to 1, with the exception of low-S/N spectra (<50), the analysis of which we do not find reliable.

To find the atmospheric parameters, we used the spectral synthesis approach, utilizing the code SPECTRUM (Gray & Corbally 1994), the MARCS grid of model atmospheres (Gustafsson et al. 2008) and solar abundances from Grevesse, Asplund & Sauval (2007). ISPEC synthesizes spectra only in certain, user-defined ranges, called ‘segments’. We followed the default approach, where these segments are defined as regions ± 2.5 Å around a certain line. We decided to synthesize spectra around a set of lines carefully selected by the the *Gaia*–ESO Survey (GES; Gilmore et al. 2012; Randich et al. 2013), in such a way that various spectral fitting codes reproduce consistent parameters from a reference solar spectrum (Blanco-Cuaresma et al. 2016).

With several exceptions, described below, we run the fit with the following parameters set be free: effective temperature T_{eff} , metallicity [M/H], alpha enhancement [α/Fe] and microturbulence velocity v_{mic} . The resolution R was always fixed to 50 000, and gravity $\log(g)$ to the value corresponding to absolute values of mass and radius (see the next section), which is more precise than $\log(g)$ we could find from spectroscopy. In case of short-period, circular (or nearly circular) orbits, where stars rotate (pseudo-)synchronously with the orbital period, the rotational velocity $v \sin(i)$ was also fixed and set to values expected from the synchronous rotation. In only three cases, we set $v \sin(i)$ to be free: KIC 7821010, 9246710 and 10031808. In the first two cases, the lines are quite narrow, so v_{mic} was automatically calculated by ISPEC from an empirical relation found by the GES Consortium and incorporated into the ISPEC program (GES Consortium, private communication). The lines of KIC 10031808 are rotationally broadened and an independent fit for v_{mic} was possible. The macroturbulence velocity v_{mac} , which

degenerates with rotation, was at all times calculated on-the-fly by ISPEC from a similar empirical relation found by the GES Consortium.

As final values of systemic [M/H] and [α/Fe], we adopted averages of values obtained from each component. As their conservative uncertainties, we added in quadrature the formal parameter errors from ISPEC and half the difference between two individual results. For example, for KIC 10031808 from $[\text{M}/\text{H}]_1 = -0.17(5)$ and $[\text{M}/\text{H}]_2 = -0.05(5)$, we obtained $[\text{M}/\text{H}] = -0.11(8)$. This particular example, and the metallicity of KIC 9641031 – i.e. $[\text{M}/\text{H}]_1 = -0.15(6)$, $[\text{M}/\text{H}]_2 = 0.00(6)$ and adopted $[\text{M}/\text{H}] = -0.07(9)$ – are the only two cases where individual values differ by more than formal 1σ , but still within 2σ . When only one component could be analysed, we adopted its [M/H] and [α/Fe] for the whole system. Abundances of specific elements were not calculated.

3.7 Calculation of absolute parameters

The partial results of LC and RV solutions were later combined in order to calculate the absolute values of stellar parameters using the JKTABSDIM code, available together with the JKTEBOP. As an input, this simple procedure takes orbital period, eccentricity, fractional radii, velocity semi-amplitudes and inclination (all with uncertainties), and returns absolute values of masses and radii (in solar units), $\log(g)$ and rotational velocities, assuming tidal locking and synchronization.

JKTABSDIM can also calculate distance to an object, using the effective temperatures of two components, the approximate metallicity (given with a precision of 0.5 dex), $E(B-V)$ and the apparent magnitudes. The code does not work on brightnesses in the *Kepler* band, so, unless stated otherwise, for the distance estimation we used B -, V -, J -, H - and K -band entries from Simbad (Wenger et al. 2000). We only used the temperatures and [M/H] from the ISPEC analysis. As the final value of distance, we adopt a weighted average of five values, calculated for each band from the surface brightness– T_{eff} relations of Kervella et al. (2004). The results can be compared with parallaxes from the *Gaia* Data Release 2 (GDR2; Prusti et al. 2016; Brown et al. 2018).

3.8 Comparison with isochrones and age estimation

We use our results to assess the age τ and evolutionary status of each system. We compare them to isochrones generated with Modules for Experiments in Stellar Astrophysics (MESA) with the aid of the MESA Isochrones and Stellar Tracks (MIST v1.2)

web interface⁷ (Paxton et al. 2011; Choi et al. 2016; Dotter 2016). To assess the age τ of a system, we searched for the best-fitting isochrone simultaneously on the M/R plane for both components, and on M/T_{eff} for one or two stars, depending on how many values of T_{eff} are known from spectroscopy. We adopt metallicities from the ISPEC analysis, and we follow the assumption used in MIST that $[\text{Fe}/\text{H}] = [\text{Z}/\text{H}]$. In its current version, MIST assumes protosolar abundance $Z = 0.0142$ from Asplund et al. (2009).

4 RESULTS

4.1 Parameters of eclipsing binaries

In this section, we present results of the combined V2FIT + JKTEBOP + ISPEC analysis of 10 double-lined eclipsing binaries, and the updated V2FIT + JKTEBOP of KIC 10191056 A, which is the close pair in a triple-lined hierarchical system. These can be found in Table 3. Observed and modelled RV and LC curves are presented in Figs 1–13.

4.1.1 KIC 3439031

This system has been observed with HIDES eight times, and has not yet been studied. It is the faintest target in our sample. We found that it is composed of two nearly identical F-type stars. Although the number of RV measurements is low, the rms of the fit is very good, and hence the mass uncertainty is also low (i.e. ~ 0.2 per cent, including systematics coming from the low number of data points).

This system has the *Kepler* short-cadence photometry available for parts of quarters Q02 and Q04, and for entire quarters Q11 and Q12. Eclipses in the short-cadence curve are deeper and last less time, meaning that the long-cadence data suffered from the longer exposure time and averaging the brightness variability. However, this system is stable out of eclipses, and we decided that the short-cadence data (presented in Fig. 1) are sufficient to analyse it properly. Furthermore, in both short- and long-cadence data we noticed that the residuals in the eclipses behaved differently from quarter to quarter; for example, the model eclipses were too shallow in long-cadence quarters Q04 and Q05, then suddenly change to being too deep in Q06 and Q07. We suspect that this is a systematic related to the rotation and orientation of the telescope. To compensate for this, we decided to analyse the LC of KIC 3439031 quarter-by-quarter and to adopt weighted averages as final values of parameters. The uncertainties were calculated with the previously described procedure that combines the rms of the results of single-quarter fits with individual errors from a MC analysis.

Apart from eclipses and ellipsoidal variations, the LC shows little variability. The rms of the fit is therefore quite low (0.33 and 0.58 mmag for long- and short-cadence curves, respectively), hampered mainly by the systematics coming from imperfect detrending and telescope's pointing stability. Final precision in the radii is at a very good level of ~ 0.15 – 0.18 per cent. The ISPEC analysis gave similar results for both components, which was expected for a pair of nearly identical stars. The system appears to be slightly more metal-rich than the Sun, and α elements are not significantly enhanced. Stars are rotating synchronously with the orbital period, and the orbit is nearly circular. The time-scale of circularization (as given by JKTABSDIM) is 4.27 Gyr, which can be treated as an upper limit of the system's age. Effective temperatures

are representative of the F6 spectral type, and are about 200 K higher than estimates from KEBC or GDR2, but this is within the error bars of our values. Disentangled spectra of higher S/N are needed to lower the uncertainties. When used in JKTABSDIM, T_{eff} gives the distance $d_J = 477(15)$ pc, which is in a reasonable agreement with 486(6) pc from GDR2. The distance calculation assumes no reddening, as the consistency between distances derived for different bands was already quite good.

The set and precision of parameters we provide for KIC 3439031, and the fact that it consists of a pair of ‘twins’, make this target valuable for testing stellar formation and evolution models.

4.1.2 KIC 4851217

A comparison of JKTEBOP output for short- and long-cadence data has shown that the two LCs are indistinguishable in shape, and the resulting parameters differ typically by less than one-fifth of the obtained errors. Therefore, we adopted the results of a fit to the complete Q00–Q17 long-cadence curve as the final ones. The long-cadence uncertainties were slightly higher (by roughly 10–20 per cent) from those of the short-cadence curve, and we decided to use them, as they are more conservative and probably better at coping with the influence of pulsations. Fig. 2 shows the long-cadence curve.

We observed this system eight times with HIDES, and additionally used three APOGEE and one TRES spectra. We did this to double-check and strengthen our orbital solution (Fig. 2), which initially disagreed with that from Matson et al. (2017). Our data clustered around phase $\phi \sim 0.3$ and in the range $\phi = 0.8$ – 1.0 . With the additional spectra, our sampling is more uniform, and the velocity amplitudes ($K_1 = 131 \pm 3$, $K_2 = 115 \pm 3$ km s $^{-1}$; Table 3) are much better constrained. The original solution from Matson et al., in which $K_1 = 115 \pm 2$, $K_2 = 107 \pm 2$ km s $^{-1}$, suffers from a similar problem (data only for $\phi = 0.25$ – 0.5 and 0.8– 0.1), which can explain the disagreement. A full comparison is shown in Table 4. A recent reanalysis of these data results in higher K (and masses), closer to our results (M. Fedurco, in preparation).

The lines are clearly broadened by rotation, which itself is synchronized with orbital period, despite the small but detectable eccentricity. Fast rotation of both components hampers our RV precision, and thus the errors in masses, which in this case are ~ 5 per cent. The precision in absolute radii is only slightly better (2–4 per cent), with error budget strongly influenced by uncertainties of fractional radii. The rms of 4.3 mmag for the LC is obviously caused by pulsations of the δSct type. In the Lomb–Scargle periodogram of the residuals of the JKTEBOP fit, we detect strong peaks at frequencies 15–21 d $^{-1}$, typical for δSct stars. A separate publication by M. Fedurco, with very detailed analysis of pulsations in KIC 4851217, is in preparation so we have not tackled this problem in this work.

Most of the flux comes from the cooler, but more massive and larger secondary. The ISPEC analysis of its spectrum ($S/N \sim 115$) showed it to be an early F-type star with $T_{\text{eff},2} = 7250(215)$ K. This is in agreement with, for example, 7300^{+225}_{-164} K from GDR2. Therefore, we expect the primary to be of spectral type A, with T_{eff} exceeding 8000 K. Unfortunately, its disentangled spectrum is not good enough for proper analysis ($S/N \sim 47$). We made several attempts to retrieve $T_{\text{eff},1}$ with ISPEC, fixing as many parameters as possible (dynamical log (g) , metallicity from secondary, etc.), and using model atmospheres appropriate for hotter stars, but we failed to reach such high temperatures. From the secondary's spectrum, we estimate the metallicity to be subsolar, and without significant α

⁷<http://waps.cfa.harvard.edu/MIST/>

Table 3. Orbital and physical parameters of 11 double-lined eclipsing binaries from our survey, including the results of spectral analysis, when possible. When ‘a’ is given in parentheses instead of uncertainty, this denotes that the parameter was calculated automatically from an empirical relation.

KIC	4851217	7821010	8552540	9246715	9641031	10031808	10191056 A	10583181	10987439	11922782
$P_{\text{orb}} (\text{d})$	5.95202634(74)	2.4702836(17)	24.238235(4)	1.06193441(4)	171.2770(6)	2.17815425(7)	8.58906432(13)	2.42749481(19)	2.696357(41)	10.67459809(33)
T_0 (JD 2454900) ^a	57.040009(11)	53.899973(53)	69.61678(13)	54.105945(27)	99.2536(31)	54.133349(3)	56.43099(10)	55.031699(5)	55.210(13)	71.885044(32)
T_P (JD 2454900) ^b	56.347(79)	54.66(27)	66.34(22)	53.846(23)	81.780(45)	53.5871(56)	56.475(74)	53.9335(11)	54.5303(34)	60.136(72)
$K_1 (\text{km s}^{-1})$	79.171(67)	131.0(2.6)	66.50(35)	121.0(1.6)	33.213(21)	93.34(10)	83.08(28)	106.96(58)	79.33(50)	76.39(10)
$K_2 (\text{km s}^{-1})$	79.274(84)	114.6(2.7)	69.55(36)	145.9(2.0)	33.629(22)	118.75(35)	80.42(15)	118.34(33)	128.81(3)	53.00(9)
$\gamma_1 (\text{km s}^{-1})$	27.023(52)	-22.9(2.2)	-17.15(46)	-14.11(1.)	-4.532(16)	-37.38(8)	12.96(17)	-25.68(23)	-40.21(2)	-19.11(11)
$\gamma_2 - \gamma_1 (\text{km s}^{-1})$	0.0(6x)	0.0(fix)	0.0(fix)	0.0(fix)	-0.05(22)	0.0(fix)	-0.17(21)	0.0(fix)	2.3(6)	-0.37(19)
q	1.0013(14)	1.143(35)	0.956(7)	0.829(16)	0.9876(9)	0.7860(23)	1.033(4)	0.9038(55)	0.6160(74)	1.4413(31)
$M_1 \sin^3(i) (\text{M}_\odot)$	1.2258(24)	1.769(88)	1.276(17)	1.144(36)	2.1782(33)	1.2056(72)	1.705(9)	1.511(12)	1.558(36)	0.9776(34)
$M_2 \sin^3(i) (\text{M}_\odot)$	1.2274(28)	2.021(94)	1.220(16)	0.948(28)	2.1512(32)	0.9477(35)	1.762(13)	1.365(15)	0.960(17)	1.4090(45)
$a \sin(i) (\text{R}_\odot)$	18.646(13)	11.99(18)	47.83(20)	5.604(54)	211.59(10)	9.134(15)	26.723(54)	10.813(32)	11.095(75)	0.829(6)
e	0.00142(16)	0.0311(7)	0.6796(16)	0.0(fix)	0.3552(4)	0.0(fix)	0.2717(14)	0.0283(23)	0.0(fix)	0.0509(14)
$\omega (\text{°})$	47(48)	188(10)	59.47(22)	-	18.22(11)	-	94.067(70)	284(4)	-	51.7(2.3)
r_1	0.07547(10)	0.1659(64)	0.02669(20)	0.2509(31)	0.0408(58)	0.1361(25)	0.09628(71)	0.1807(19)	0.1696(6)	0.03409(54)
r_2	0.07524(13)	0.2607(32)	0.02530(27)	0.1806(40)	0.03870(40)	0.0984(26)	0.11250(47)	0.1517(27)	0.0883(7)	0.0704(52)
$i (\text{°})$	89.57(1)	77.1(26)	89.58(2)	85.83(46)	87.04(31)	87.13(71)	83.323(47)	81.33(8)	89.4(8)	85.614(66)
J	0.9970(26)	0.9324(43)	0.9222(23)	0.67(14)	1.0424(49)	0.396(49)	0.903(34)	0.945(9)	0.411(14)	0.46(11)
I_2/I_1	0.9933(51)	2.32(23)	0.83(4)	0.2921(10)	0.964(48)	0.224(35)	1.2303(23)	0.68(4)	0.0(fix)	0.0(fix)
I_3/I_{tot}	~0.0(var)	0.0(fix)	0.0(fix)	0.0(fix)	0.0(fix)	0.0(fix)	0.0(fix)	0.0(fix)	~0.12(var)	0.0(fix)
$M_1 (\text{M}_\odot)$	1.2259(24)	1.91(10)	1.277(17)	1.153(36)	2.1869(33)	1.2102(76)	1.741(9)	1.564(12)	1.559(36)	1.067(10)
$M_2 (\text{M}_\odot)$	1.2275(28)	2.18(10)	1.221(16)	0.956(28)	2.1598(32)	0.9512(39)	1.798(13)	1.413(16)	0.960(16)	1.4215(45)
$R_1 (\text{R}_\odot)$	1.4072(22)	2.04(85)	1.276(11)	1.410(22)	8.49(12)	1.244(23)	2.590(20)	1.976(22)	1.882(14)	0.932(15)
$R_2 (\text{R}_\odot)$	1.4030(25)	3.207(63)	1.210(14)	1.015(24)	8.20(9)	0.900(24)	3.027(14)	1.659(30)	0.980(10)	1.512(31)
$a (\text{R}_\odot)$	18.646(13)	12.30(19)	47.83(20)	5.619(54)	211.87(10)	9.145(16)	26.905(54)	10.938(33)	11.095(75)	27.352(29)
$\log(g_1)$	4.2300(13)	4.100(35)	4.332(27)	4.202(12)	2.920(13)	4.331(16)	3.852(6)	4.041(9)	4.082(5)	4.493(14)
$\log(g_2)$	4.2332(15)	3.765(13)	4.359(9)	4.406(20)	2.945(9)	4.508(23)	3.731(4)	4.149(16)	4.438(7)	4.232(18)
$T_{\text{eff},1} (\text{K})$	6530(220)	-	6720(160)	6060(200)	4890(50)	6260(120)	7105(110)	-	6730(140)	-
$T_{\text{eff},2} (\text{K})$	6530(220)	7250(215)	6570(190)	-	4905(60)	5490(240)	6840(105)	-	6490(90)	-
$\log(L_1)(L_\odot)$	0.45(6)	-	0.47(4)	0.381(59)	1.567(22)	0.320(35)	1.185(27)	-	0.824(37)	-
$\log(L_2)(L_\odot)$	0.45(6)	1.406(54)	0.39(5)	-	1.543(22)	-0.180(80)	1.254(27)	-	0.550(30)	-
$v_{\text{rot},1} (\text{km s}^{-1})^c$	11.96(2.8)	41.8(1.7)s	1.3(4.8)	67.1(1.0)s	2.56(22)	28.89(54)s	14.9(1.1)	41.2(5)s	35.31(26)s	4.427(7)s
$v_{\text{rot},2} (\text{km s}^{-1})^c$	11.92(2.8)	65.7(1.3)s	8.9(1.1)	48.3(1.2)s	2.63(22)	20.89(55)s	10.2(2.0)	34.6(6)s	18.39(19)s	7.16(15)s
$v_{\text{mic},1} (\text{km s}^{-1})$	1.63(21)	-	1.54(a)	1.28(40)	1.27(a)	1.90(18)	2.76(25)	-	2.20(27)	-
$v_{\text{mic},2} (\text{km s}^{-1})$	1.72(21)	1.70(47)	1.44(a)	-	1.27(a)	1.79(54)	3.26(31)	-	1.88(21)	-
$v_{\text{mac},1} (\text{km s}^{-1})^c$	9.24(a)	-	11.13(a)	5.99(a)	3.83(a)	7.23(a)	13.01(a)	-	11.46(a)	-
$v_{\text{mac},2} (\text{km s}^{-1})^c$	9.29(a)	18.4(a)	9.56(a)	-	3.77(a)	3.33(a)	16.21(a)	-	8.97(a)	-
$[\text{M}/\text{H}]$	0.10(3)	-0.08(9)	0.10(8)	-0.27(11)	0.01(3)	-0.07(9)	-0.11(8)	-	-0.01(7)	-0.03(5)
$[\alpha/\text{Fe}]$	0.03(14)	-0.03(15)	-0.01(11)	-0.01(3)	0.03(9)	0.16(6)	-	0.00(7)	0.05(16)	-0.01(6)
$d_1 (\text{pc})^d$	477(15)	-	342(13)	-	573(13)	130(5)	445(15)	-	-	5.57(a)
$\text{rmsRV} (\text{km s}^{-1})$	0.15	3.80	0.092	3.02	0.046	0.39	0.50	1.70	0.70	0.129
$\text{rmsRV2} (\text{km s}^{-1})$	0.17	4.82	0.217	5.26	0.051	0.83	1.08	2.50	0.042	1.02
$\text{rmsLC} (\text{mmag})^e$	0.36	4.25	0.50	12.7	0.61	5.44	1.22	0.41	2.06	0.072
$\text{rmsSC} (\text{mmag})^e$	0.58	5.13	0.45	14.6	-	5.50	1.26	0.40	1.69	5.60

^aMid-time of the primary (deeper) eclipse, calculated from the complete Q0–Q17 curve.

^bTime of pericentre or quadrature.

^cIf ‘s’ is given after the uncertainty, it is the velocity of (pseudo-)synchronous rotation given by JKTABSDIM. Otherwise, it is $v \sin(i)$ calculated by ISPEC.

^dThe JKTABSDIM distance d_1 is calculated only when both values of T_{eff} were found with ISPEC.

^eThe rms of residuals of the fit to the complete long-cadence (LC) and short-cadence (SC) Kepler curve.

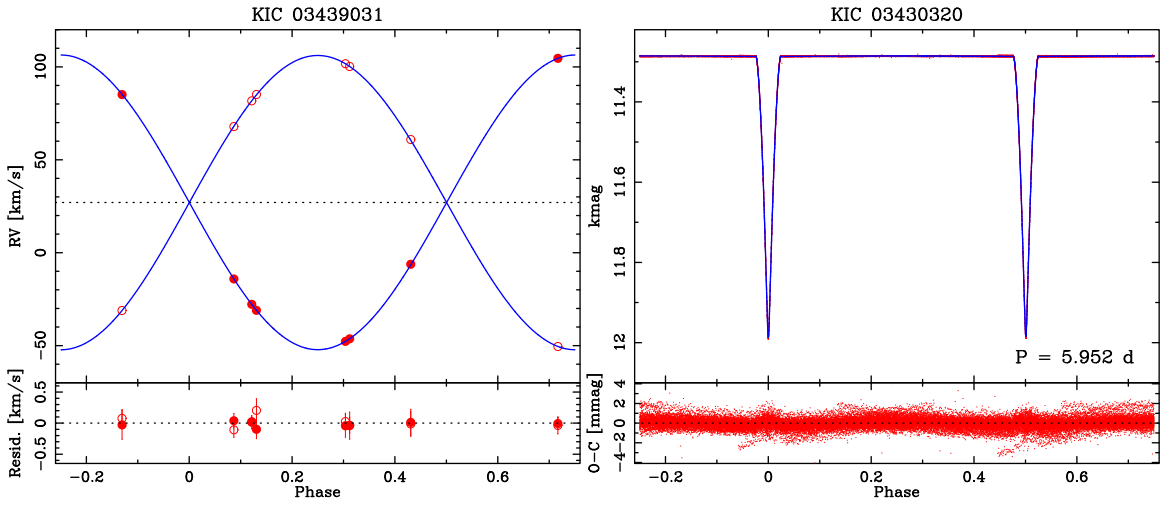


Figure 1. RV curves (left) and LCs (right) of KIC 3439031. The best-fitting models are plotted with blue lines. Filled circles on the RV plot refer to HIDES data for the primary, and open circles to the secondary. In both panels, the phase 0 is set for the deeper eclipse mid-time, according to the definition in JKTEBOP.

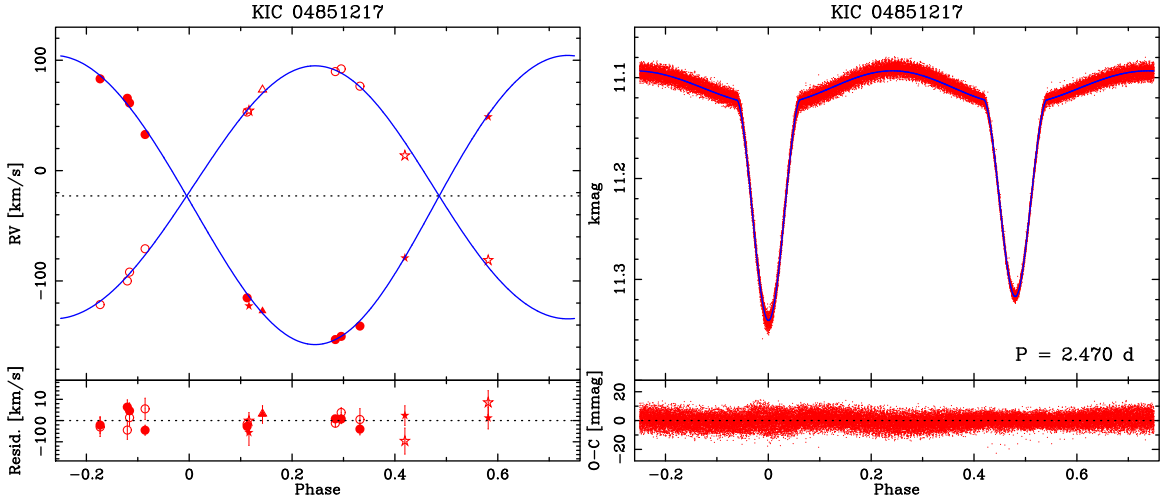


Figure 2. Same as Fig. 1, but for KIC 4851217 and with additional RV measurements from APOGEE (stars) and TRES (triangles).

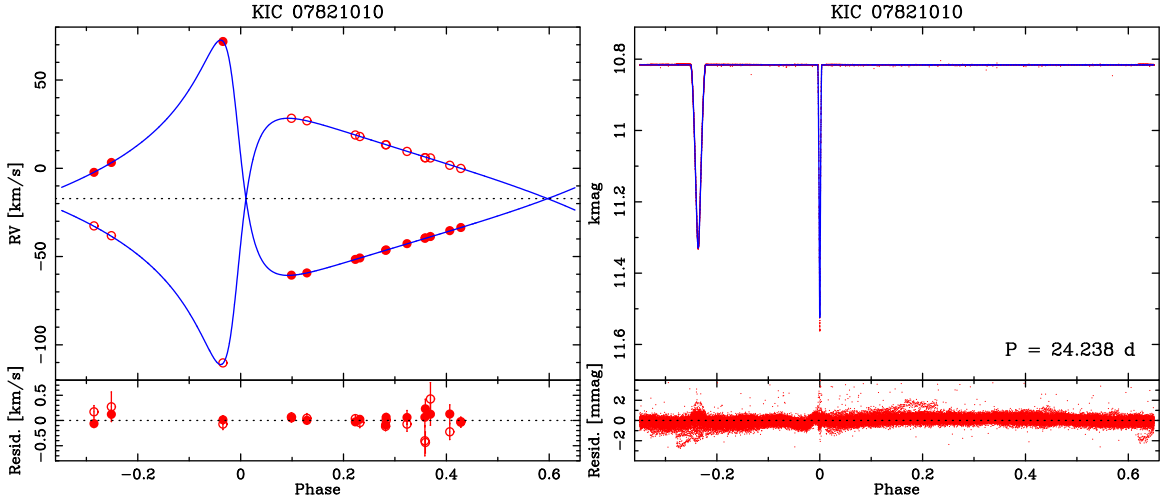


Figure 3. Same as Fig. 1, but for KIC 7821010.

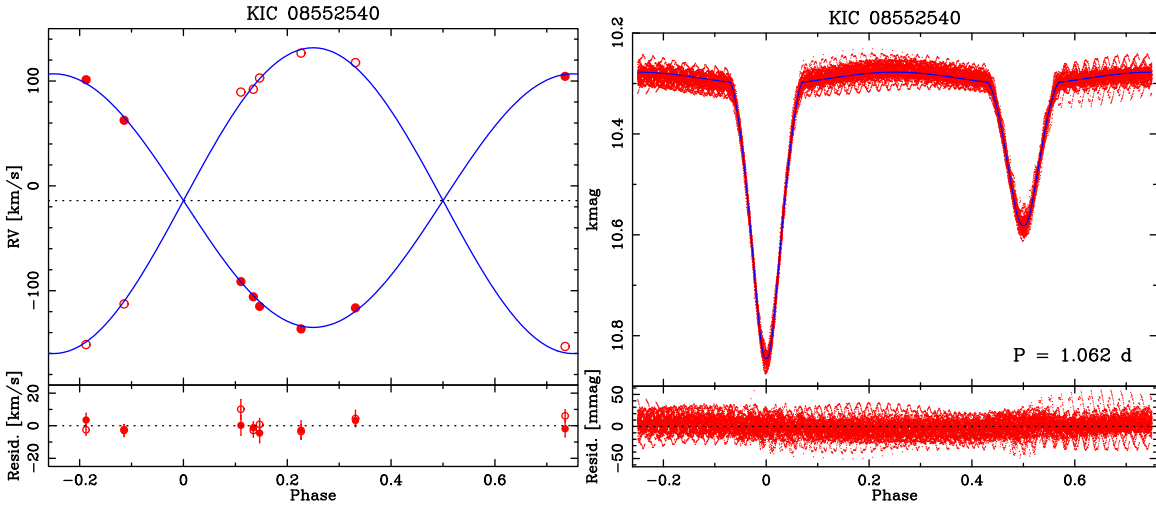


Figure 4. Same as Fig. 1, but for KIC 8552540.

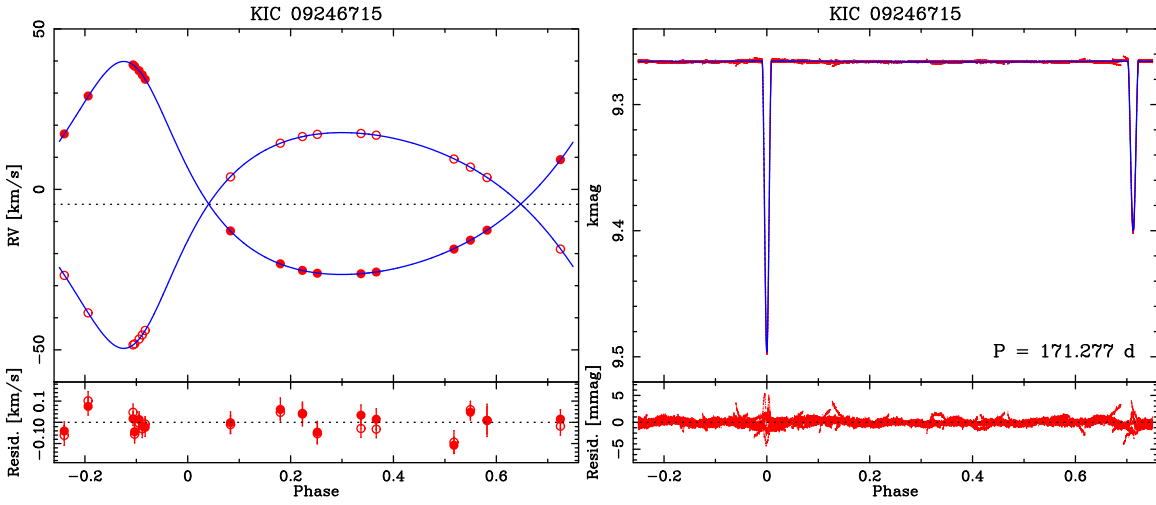


Figure 5. Same as Fig. 1, but for KIC 9246715.

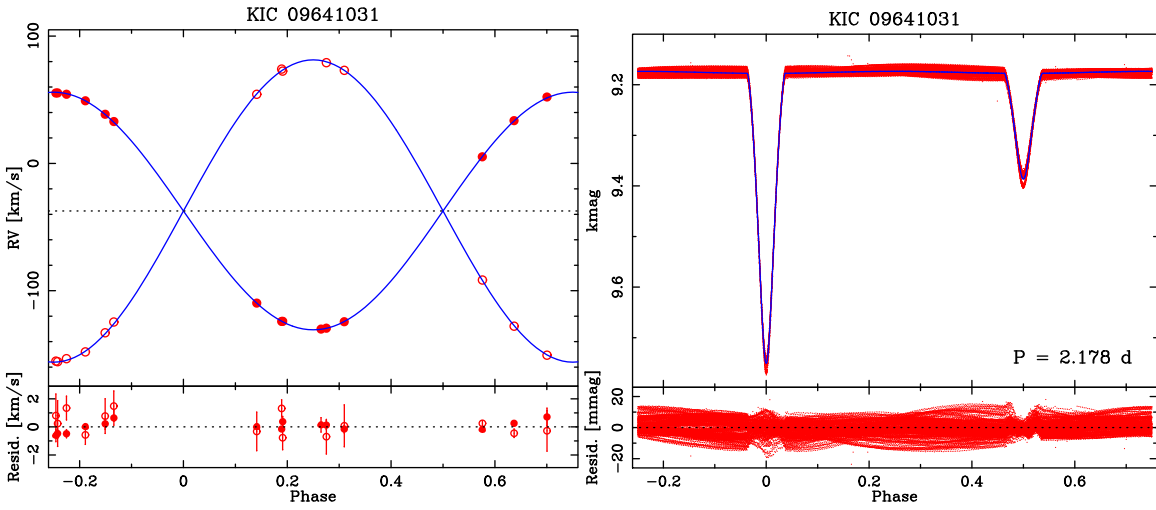


Figure 6. Same as Fig. 1, but for KIC 9641031.

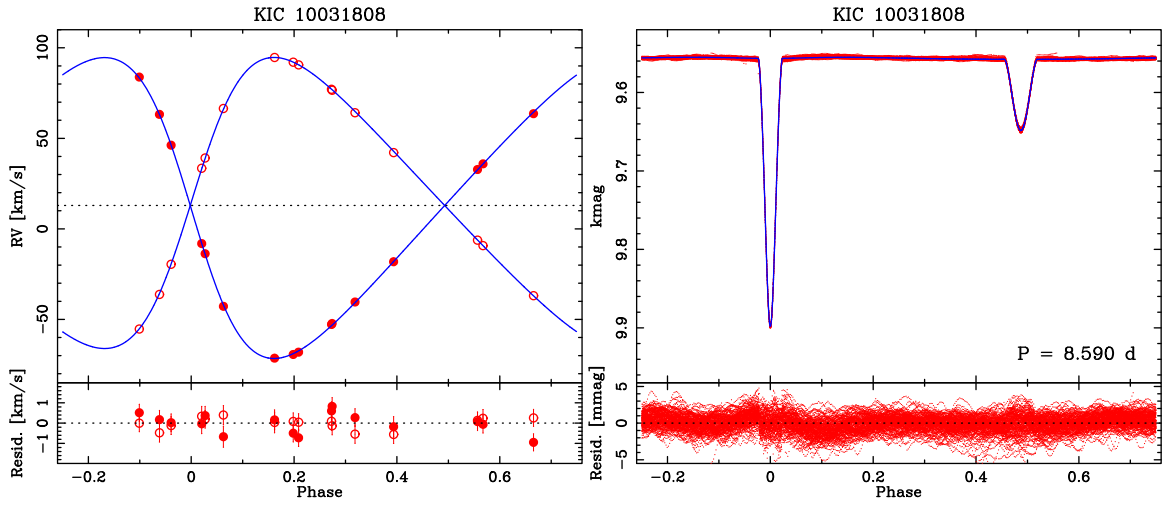


Figure 7. Same as Fig. 1, but for KIC 10031808.

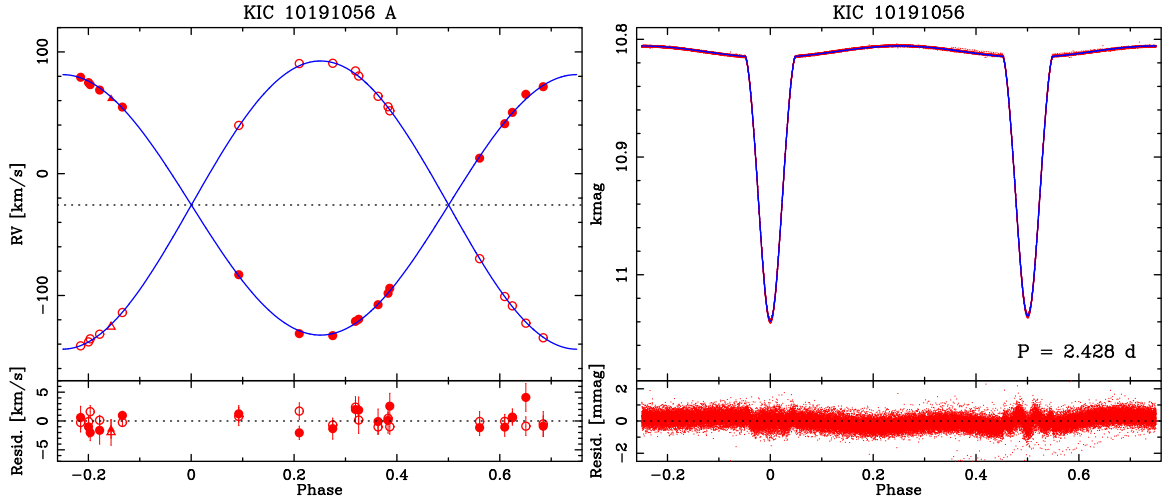


Figure 8. Same as Fig. 1, but for KIC 10191056 A and RV measurements from TRES (triangles).

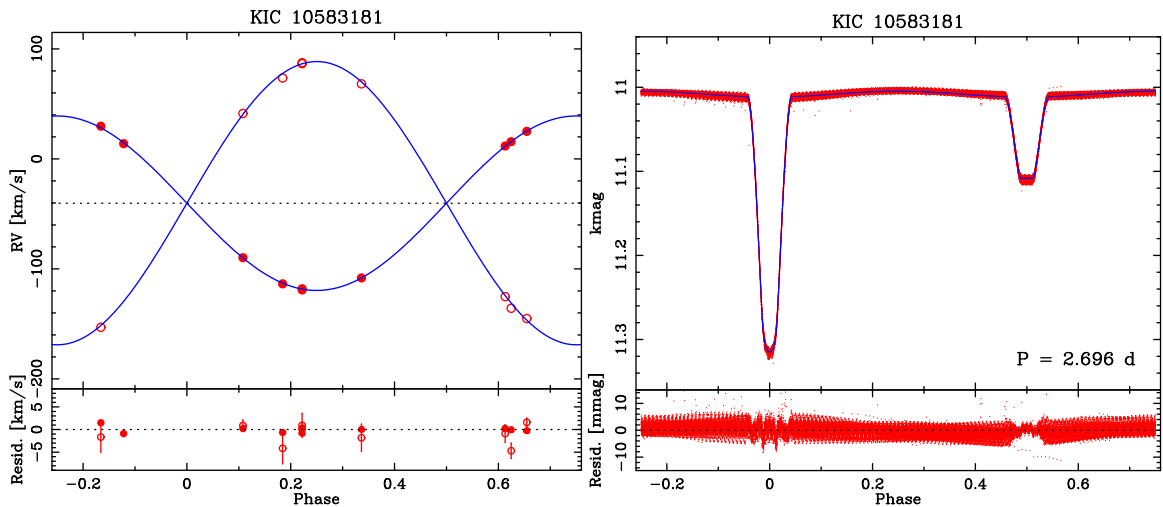


Figure 9. Same as Fig. 1, but for KIC 10583181. The RV modulation coming from the circumbinary body has been removed.

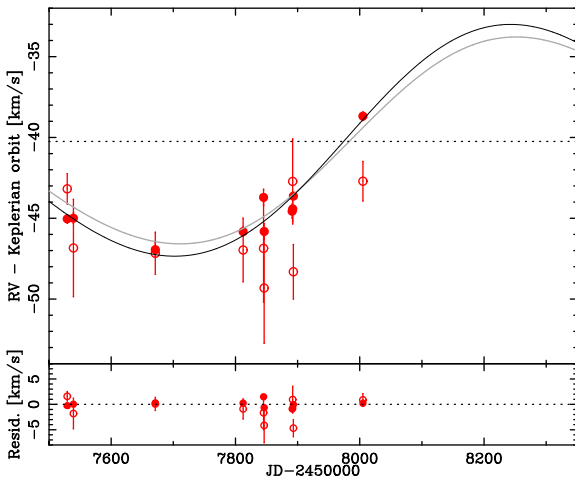


Figure 10. RVs of KIC 10583181 as a function of time after removing the inner Keplerian orbit. Symbols are the same as in Fig. 9. The black line is the best-fitting model of centre-of-mass velocity γ variation. The grey line is γ variation predicted by the exact solution from Borkovits et al. (2016). The plot is stretched to JD = 245 8350 to show the total scale of velocity variation.

enhancement. Without independent assessment of $T_{\text{eff},1}$, we cannot estimate the distance using JKTABSDIM. We do this in Section 4.2 on the basis of isochrone-calibrated $T_{\text{eff},1}$.

4.1.3 KIC 7821010

This system has been reported on several occasions to harbour a circumbinary planet, detected with ETVs⁸ (Borkovits et al. 2016), but a proper study of the system has not yet been published (Fabrycky et al., in preparation). Since the publication of Paper II, we have obtained seven HIDES spectra of the system. We have previously reported the uneven quality of the data, and we have shown that, with favourable observing conditions, our observations result in a sufficient S/N to obtain good precision RV measurements ($<100 \text{ m s}^{-1}$). New observations aim to increase the number of ‘good’ spectra, to improve the precision of absolute stellar parameters and, possibly, to detect the RV signature of the planet, estimated from the solution of Borkovits et al. (2016) to be $30\text{--}40 \text{ m s}^{-1}$, which is at the level of instrumental precision in our programme (Paper I). For the new orbital solution, we did not use RVs coming from one of the older spectra, from 2015 May 05 (JD $\simeq 245\,7148.2$), which had very low S/N (<15). Therefore, the final solution, and spectra disentangling, was based on 15 observations. The resulting TD spectra are of a good quality (S/N = 127 and 108 for the primary and secondary, respectively).

The short-cadence *Kepler* photometry of this pair is available from Q02 and Q09–Q17 (nine quarters). When comparing the LCs, we found that the eclipses in the long-cadence LC are slightly shallower and wider, likely because short-time-scale brightness variations were averaged out with the longer exposure time. For this reason, our results are based on the short-cadence data only. We do not see significant out-of-eclipse variations, but we see the influence of the circumbinary planet on T_0 and P in each quarter. The fit to a complete LC left characteristic residuals around eclipses,

and therefore we adopted the weighted averages from single-quarter fits. In Fig. 3, we present the short-cadence LC, but the lower panel shows summarized residuals of single-quarter fits. Some systematic residuals, coming from imperfect de-trending, are clearly visible.

Mass uncertainties in the new solution (Table 3) are about one-third lower than in Paper II (~ 0.8 per cent for both components), and, because of the improved $a \sin(i)$, the uncertainty in radii is also good (0.8 and 1.1 per cent for the primary and secondary, respectively). The rms of the orbital fit also decreased. With the selection of only the best RV measurements (10 for the primary and 8 for the secondary), we can lower it even further, to 55 and 60 m s^{-1} , respectively. This is, unfortunately, larger than the expected RV signal from the planet. While attempting to fit for this influence, based on the orbital parameters from Borkovits et al. (2016), we obtained a solution that was only marginally better (rms of $52 + 55 \text{ m s}^{-1}$).

The ISPEC analysis resulted in similar effective temperatures of the components, which is not surprising considering a mass ratio slightly lower than 1. The system’s metallicity is likely higher than solar, that is, $+0.10(8)$ dex, with two individual results being different by only 0.01 dex. We found no evidence for enhancement of α -elements in either component. With ISPEC, we also fitted for the projected rotational velocities $v \sin(i)$. The lines of both components are narrow, but some degree of broadening was expected for the secondary (from the width of the cross-correlation function). Indeed, we found the secondary rotating faster ($8.9 \pm 1.1 \text{ km s}^{-1}$) than expected in the pseudo-synchronous case ($2.53 \pm 0.03 \text{ km s}^{-1}$). The formal error of the primary’s $v \sin(i)$ is larger than the best-fitting value of $1.3 \pm 4.8 \text{ km s}^{-1}$, so the result is inconclusive. However, from the secondary alone, we can conclude that KIC 7821010 did not reach the tidal equilibrium. Therefore, KIC 7821010 should be younger than 3.6 Gyr, which is the time-scale of synchronization of rotation with orbital period (from JKTABSDIM).

The two effective temperatures were used in JKTABSDIM to estimate the distance d_J . The result, that is, $342(13)$ pc, is in reasonable agreement with $360(5)$ pc from GDR2. To ensure the consistency between individual distances from various bands, we assumed $E(B - V) = 0.11$ mag. Without reddening, values corresponding to bands B and V are ~ 60 pc larger than those corresponding to J , H and K . The equivalent width of the interstellar sodium D1 line is $0.21(1)$ Å, and correctly reproduces $E(B - V) \simeq 0.11$ mag, according to calibrations by Munari & Zwitter (1997).

4.1.4 KIC 8552540 (V2277 Cyg)

The LC of this system is affected greatly by rapidly evolving spots. Short-cadence data are available only for fractions of quarters Q02, Q03 and Q14, and these are not enough to cover the evolution of spots properly and to obtain reliable results. Therefore, we use the fit to a complete Q00–Q17 long-cadence curve (shown in Fig. 4), with uncertainties calculated with our RS approach (i.e. the results from Paper II remain intact). For the record, we also give the rms of the best fit to the short-cadence LC.

Furthermore, this system has no new HIDES observations, so the only new addition is the ISPEC spectroscopic analysis. Like KIC 4851217, this binary also has a large ratio of component fluxes, and significantly different S/Ns of disentangled spectra: 136 and 37 for the primary and secondary, respectively. It is the shortest-period binary in our sample, with two rapidly rotating components, and therefore the final mass precision is relatively poor (~ 3 per cent). The rapidly evolving spots affect the precision of the LC

⁸See, for example, <http://www.astro.up.pt/investigacao/conferencias/toe2014/files/wwelsh.pdf>.

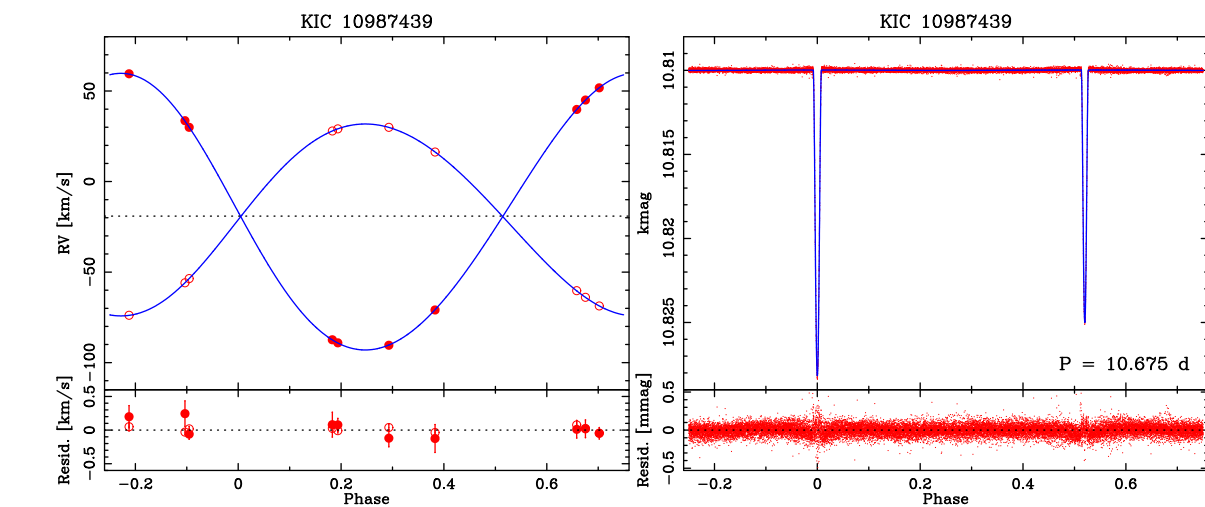
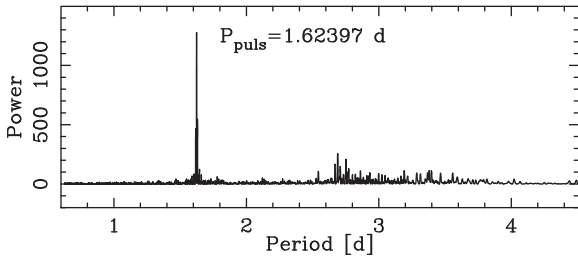


Figure 11. Same as Fig. 1, but for KIC 10987439.

Figure 12. Lomb-Scargle periodogram of residuals of our JKTEBOP fit to the *Kepler* long-cadence curve of KIC 10987439. The detected periodicities, with the dominant one at 1.624 d, suggest γ Dor-type pulsations.

fit (the largest $\text{rms}_{\text{LC}} \simeq 13$ mmag). It is worth noting that the secondary can be considered a solar analogue. It has also been reported in Matson et al. (2017), and a comparison is shown in Table 5. There is an overall agreement, except for K_2 . This is not very surprising, considering the low precision of RV measurements of the faint and rotationally broadened secondary, which affected both studies.

The ISPEC analysis of the primary's spectrum was carried out using $v \sin(i)$ fixed to the value predicted by tidal locking. We found $[\text{M}/\text{H}] = -0.27(11)$ dex (the lowest in our sample), no significant α -element enhancement and $T_{\text{eff},1} = 6060(200)$ K. This agrees with 5870^{+290}_{-118} K from GDR2. Because of the strong rotational broadening of lines, the uncertainties are relatively large. The spectrum of the secondary had its S/N too low for secure analysis, so without $T_{\text{eff},2}$ we are not able to calculate the distance with JKTABSDIM at this stage. Attempts made on isochrone-based values are described in Section 4.2.

4.1.5 KIC 9246715

This system was previously described in a dedicated paper (K924), and since then it has been observed nine more times with HIDES, making the total number of spectra 17. No *Kepler* short-cadence data are available. Except for eclipses, the long-cadence curve shows systematics, presumably coming from imperfect de-trending, also affecting some of the eclipses (Fig. 5). It should be noted that the long period of this system (171 d) means that both minima are not

always recorded during one quarter. The approach to the LC fit was therefore slightly different, and this is described in detail in K924. We do not repeat the LC analysis here.

KIC 9246715 is one of the most interesting cases in our sample. It is composed of two red giants, one of which shows solar-type oscillations. At the time of publication, it was only the third example of a Galactic double-giant eclipsing binary with masses and radii measured with precision below 2 per cent. It was simultaneously and independently analysed by Rawls et al. (2016), who used their own set of 24 high-resolution spectra (from TRES, ARCES and APOGEE) and derived parameters in agreement with K924. A comparison of these results with K924 and this work is shown in Table 6. The full set of our parameters is presented in Table 3. Additionally, Rawls et al. (2016) estimated temperatures and iron abundance from the disentangled component spectra, analysed pulsations and compared the binary with models. They concluded that one of the components is in a helium (He) burning phase.

The fact that KIC 9246715 contains a solar-type oscillator makes it useful for testing and calibrating asteroseismic relations (Gaulme et al. 2016; Brogaard et al. 2018). The analysis of oscillations is dependent on the evolutionary status of a star, which requires very precise observables to be securely established. It should be noted that in K924 there were only eight RV measurements used, and the resulting precision of $K_{1,2}$ suffered severely because of this, even though the rms of the orbital fit was only ~ 50 m s $^{-1}$ (close to the stability level of HIDES in our survey; Paper I). Also, the spread of RV residuals in Rawls et al. (2016, see their fig. 6) reaches ± 2 km s $^{-1}$, suggesting that the rms is of the order of a few hundred m s $^{-1}$, and it clearly shows systematic effects (residuals for one component strongly correlated with the other). It is therefore likely that their uncertainties of $K_{1,2}$ (40 – 50 m s $^{-1}$) are underestimated, as are the errors of masses. We followed KIC 9246715 in order to improve the orbital, and therefore the physical parameters of its components.

We doubled the number of HIDES spectra, but the quality of the orbital fit remained almost unchanged. With more data and better sampling, we reduced the systematics in velocity amplitudes $K_{1,2}$, and also improved our estimate of eccentricity, which, as it turns out, has a large influence on the final errors of masses. The final precision is ~ 0.15 per cent for both components. The precision in R

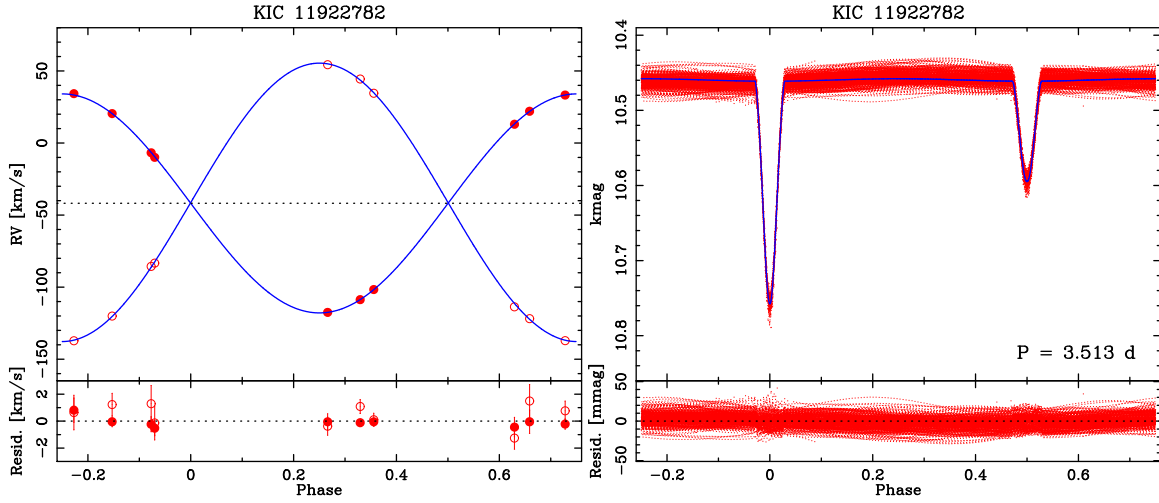


Figure 13. Same as Fig. 1, but for KIC 11922782.

Table 4. Comparison of updated results for KIC 4851217 with parameters from Matson et al. (2017).

Parameter	This work (Table 3)	Matson et al. (2017)
P (d)	2.4702836 (17)	2.47028283 (–)
K_1 (km s $^{-1}$)	131.0 (2.6)	115 (2)
K_2 (km s $^{-1}$)	114.6 (2.7)	107 (2)
q	1.143 (35)	1.08 (3)
i ($^{\circ}$)	77.11 (26)	77.8 (–)
a (R_{\odot})	12.30 (19)	11.1 (2)
M_1 (M_{\odot})	1.19 (10)	1.43 (5)
M_2 (M_{\odot})	2.18 (10)	1.55 (5)
rms ₁ (km s $^{-1}$)	3.8	7.0
rms ₂ (km s $^{-1}$)	4.8	7.2

Table 5. Comparison of our results for KIC 8552540 (V2277 Cyg) with parameters from Matson et al. (2017).

Parameter	This work ^a (Table 3)	Matson et al. (2017)
P (d)	1.06193441(4)	1.06193426(–)
K_1 (km s $^{-1}$)	121.0(1.6)	121(1)
K_2 (km s $^{-1}$)	145.9(2.0)	153(2)
q	0.829(16)	0.79(1)
i ($^{\circ}$)	85.83(46)	80.7(–)
a (R_{\odot})	5.619(54)	5.83(5)
M_1 (M_{\odot})	1.153(36)	1.32(3)
M_2 (M_{\odot})	0.956(28)	1.04(2)
rms ₁ (km s $^{-1}$)	3.0	4.1
rms ₂ (km s $^{-1}$)	5.3	6.3

^aThe same as in Paper II.

is $1.4 + 1.0$ per cent, analogously. Results for radii did not change much, as we did not reanalyse the LC.

Both disentangled spectra have decent S/N (123 and 117), and their ISPEC analysis gave similar temperatures of components: 4890(50) and 4905(60) K for the primary and secondary, respectively. Individual values of [M/H] and $[\alpha/\text{Fe}]$ were in good agreement, and pointed towards a chemical composition indifferent from solar. Rotational velocities $v \sin(i)$ were fitted for, and we

Table 6. Comparison of updated results for KIC 9246715 with parameters from K924 and Rawls et al. (2016).

Parameter	This work (Table 3)	K924 (Table 2)	Rawls et al. (2016)
P (d)	171.2770(6)	171.27688(1)	171.27688(1)
K_1 (km s $^{-1}$)	33.21(2)	33.18(16)	$33.19^{+0.04}_{-0.05}$
K_2 (km s $^{-1}$)	33.63(2)	33.58(14)	$33.53^{+0.04}_{-0.05}$
e	0.3552(4)	0.3587(9)	$0.3559^{+0.0002}_{-0.0003}$
r_1	0.04008(58)	0.0396 $^{+0.0001}_{-0.0003}$	0.0396 $^{+0.0001}_{-0.0003}$
r_2	0.03870(40)	0.0393(1)	0.0393(1)
i ($^{\circ}$)	87.049(31)	87.051 $^{+0.009}_{-0.003}$	87.051 $^{+0.009}_{-0.003}$
M_1 (M_{\odot})	2.187(3)	2.169(24)	$2.171^{+0.006}_{-0.008}$
M_2 (M_{\odot})	2.160(3)	2.143(25)	$2.149^{+0.006}_{-0.008}$
R_1 (R_{\odot})	8.49(12)	8.47(13)	$8.37^{+0.03}_{-0.07}$
R_2 (R_{\odot})	8.20(9)	8.18(9)	$8.30^{+0.04}_{-0.03}$
$T_{\text{eff},1}$ (K)	4890(50)	–	4990(90)
$T_{\text{eff},2}$ (K)	4905(55)	–	5030(80)
[M/H] ₁	-0.01(2)	–	-0.22(12) ^a
[M/H] ₂	0.03(2)	–	-0.10(9) ^a
rms _{rv1} (km s $^{-1}$)	0.046	0.045	0.55 ^b
rms _{rv2} (km s $^{-1}$)	0.051	0.052	0.55 ^b

^a[Fe/H] obtained with MOOG.

^bNot given directly in Rawls et al. (2016), so it was calculated in this work with v2FIT using their exact solution.

found them to be in very good agreement with those predicted by pseudo-synchronization: 2.51(4) and 2.42(3) km s $^{-1}$ (from JKTABSDIM). It is, however, unlikely that at such separation tidal forces influenced the rotation and synchronized it with the orbital period during the lifetime of the system. The observed rotation is rather primordial.

We used JKTABSDIM and our values of T_{eff} to estimate the distance. We found it to be 573(13) pc, assuming $E(B - V) \simeq 0.13$ mag, which is significantly less than 616(11) pc from GDR2. When no reddening is assumed, individual distances in B and V are larger from those in J , H and K by ~ 150 and 100 pc, respectively. The infrared values themselves are all around 600 pc, still too low for GDR2.

Table 7. Comparison of updated results for KIC 9641031 (FL Lyr) with parameters from Paper II and Popper et al. (1986).

Parameter	This work (Table 3)	Paper II (Table 2)	Popper et al. (1986)
P (d)	2.17815425(7)	2.1781542(3)	
K_1 (km s^{-1})	93.34(10)	93.23(12)	93.5(5)
K_2 (km s^{-1})	118.75(35)	118.19(30)	118.9(7)
r_1	0.1361(25)	0.1389(25)	0.140(3)
r_2	0.0984(26)	0.0995(27)	0.105(3)
i ($^\circ$)	87.13(71)	85.36(71)	86.3(4)
M_1 (M_\odot)	1.2102(76)	1.2041(76)	1.218(16)
M_2 (M_\odot)	0.9512(39)	0.9498(46)	0.958(11)
R_1 (R_\odot)	1.244(23)	1.269(23)	1.283(30)
R_2 (R_\odot)	0.900(24)	0.908(24)	0.963(30)
$T_{\text{eff},1}$ (K)	6264(112)	–	6150(100)
$T_{\text{eff},2}$ (K)	5490(247)	–	5300(100)
[M/H]	-0.07(9)	–	0.32(–)

4.1.6 KIC 9641031 (FL Lyr)

This binary has a very extensive set of short-cadence data points, starting in quarters Q01 and Q02, through almost the entire quarters Q07 and Q08, and with a nearly continuous coverage since Q13 until the end of the mission. In this case, we also noted slightly different eclipse depths in short- and long-cadence data. Therefore, the final values come from a fit to a complete short-cadence curve (see Fig. 6), although the long-cadence curve gives similar results. However, both components of this pair seem to have prominent, rapidly evolving spots, which make the shape of the LC change in relatively short time-scales (a significant change is seen after only several orbits). The complete long-cadence LC, whose coverage in time is much more complete,⁹ seems to probe the evolution of spots more uniformly, and their influence on the phase-folded LC appears to be averaged out. This type of situation favours the RS method over the MC for error determination, so the uncertainties quoted in Table 3 come from the combined RS + rms analysis of single-quarter long-cadence data.

We have observed this system with HIDES three more times since Paper II, increasing the number of spectra to 15 (14 of which were used in TD). The new data were taken mainly to test the hypothesis of a low-mass circumbinary body on a 103-d orbit, based on ETVs from Paper II. We do not detect any RV modulation at the expected level ($\sim 1.26 \text{ km s}^{-1}$), so we conclude that the observed ETVs were likely caused by the evolution of spots. The overall precision of RV data and the level of uncertainties are similar to those from Paper II (0.5–0.7 per cent in mass and 1.8–2.6 per cent in radii). In principle, compared with the previous extensive study of this system by Popper et al. (1986), we reach errors in mass that are two to three times lower, and comparable errors in radii (though slightly lower). To decrease errors of R , we would have to remove the influence of spots on the LC. However, for this, knowledge about their location (i.e. which component is affected) is required, in order not to hamper the depths of the eclipses. Rapid evolution of spots on this system makes such an analysis quite challenging.

Our updated parameters are in better agreement with Popper et al. (1986) than with Paper II, due to larger K_2 . Direct comparison is presented in Table 7. We now also add effective temperatures and metallicity of KIC 9641031, obtained from spectra. Popper et al. estimated T_{eff} from the $V - R$ colours from their photometric

solution and on the basis of calibrations from Popper (1980), and metal content $Z = 0.04$ from comparison with isochrones on the mass–temperature plane. They also admit that not all uncertainties were included in temperature errors. Our T_{eff} estimates from ISPEC are in formal agreement (due to error bars) but both are larger. When compared with a modern calibration, from Worthey & Lee (2011), the adopted $V - R$ indices (0.46 and 0.61 mag for the primary and secondary, respectively) actually predict temperatures about 1000 K lower, or themselves are 0.15 mag too high. We should also note that the calibrations from Popper (1980) played a role in establishing the ratios of radii k and fluxes in Popper et al. (1986). Our approach is calibration-independent, and resulted in different values of k and (subsequently) R_2 . The issue with the uncertainties of r and R in Popper et al. (1986) was already raised in Paper II. For these reasons, we advise that the results from Popper et al. (1986) should be treated with caution. The difference in metallicity is discussed in Section 4.2.

The temperatures from Table 3 were used to estimate the distance with JKTABSDIM . The resulting value of 130(5) pc is in good agreement with 135.0(5) pc from GDR2, but a small amount of reddening, $E(B - V) = 0.04$ mag, had to be assumed to reach consistency between distances from the B and V bands with those from J , H and K . Without reddening, the B and V distances were systematically larger by 5–10 pc.

4.1.7 KIC 10031808

In the LC analysis of KIC 10031808, we did not use short-cadence data, as these are only available for a fraction of quarter Q02. In general, the shapes and depths of eclipses agree in both short- and long-cadence photometry. Fig. 7 depicts the long-cadence curve, and the final parameters were taken from a fit to a complete Q00–Q17 set (i.e. the results presented in Paper II remain unchanged).

This system has no new HIDES observations since Paper II, but it is one of the most interesting targets in the sample. It contains a γ Dor-type pulsator, and it is one of only a few known cases of such a star in an eclipsing binary with precisely measured parameters (i.e. 0.4–0.8 per cent in both masses and radii). The DEBCat lists only two systems with γ Dor stars: CoRoT 102918586 (Maceroni et al. 2013) and KIC 11285625 (Debosscher et al. 2013). There are, of course, other known cases, but they do not have parameters derived with sufficient precision. Comparison of our values of T_{eff} , $\log(g)$ and v_{mic} of both components with the distributions of those parameters in Kahraman Aliçavuş et al. (2016) suggests that the $1.74 \cdot M_\odot$ primary is the pulsator. In particular, in Kahraman Aliçavuş et al. (2016), there is no case of a γ Dor pulsator with $\log(g)$ lower than 3.8 dex.

We found the metallicity of this system to be slightly sub-solar (-0.11 ± 0.08 dex), but both components show a clear α -enhancement (0.16 ± 0.06 dex). The obtained effective temperatures are close to those predicted in Paper II, but the resulting $d_1 = 445(15)$ pc is only in a $\sim 2\sigma$ agreement with the one from GDR2. Our distance estimate assumes $E(B - V) = 0.125$ mag, which is required to obtain consistency between the distances calculated for each band. A better match with GDR2 is found when $E(B - V) \simeq 0.08$ mag but, in such a case, distances from B and V bands are systematically larger than those from J , H and K by about 30 pc. The equivalent width of the sodium D1 line is $0.43(5)$ Å, and, according to calibrations from Munari & Zwitter (1997), favours the value of $E(B - V) = 0.125$ mag.

⁹There are no *Kepler* data from Q04.

Table 8. Comparison of updated results for KIC 10191056 with parameters from Paper II and Matson et al. (2017).

Parameter	This work (Table 3)	Paper II (Table 2)	Matson et al. (2017)
P (d)	2.42749488(2)	2.42749484(–)	
K_1 (km s^{-1})	106.96(58)	107.0(1.3)	100(2)
K_2 (km s^{-1})	118.34(33)	119.3(1.0)	119(2)
q	0.9038(55)	0.897(13)	0.83(2)
i ($^\circ$)	81.33(8)	81.35(8)	80.5(–)
a (R_\odot)	10.938(33)	10.986(80)	10.7(2)
M_1 (M_\odot)	1.564(12)	1.590(32)	1.50(5)
M_2 (M_\odot)	1.413(16)	1.427(36)	1.25(4)
rms_{RV1} (km s^{-1})	1.7	2.5	6.8
rms_{RV2} (km s^{-1})	1.1	2.3	6.9

4.1.8 KIC 10191056 A

The triple-lined KIC 10191056 has been observed eight additional times since Paper II, but here we have not used the low-S/N spectrum taken on 2016 October 10 (JD $\simeq 254\,7671.97$), so the total number of HIDES spectra is 18. The main goal was to monitor the variations of systemic velocity γ of the eclipsing pair A, and the motion of the tertiary B, which is described in detail in Section 4.3. The TRES spectrum was included in this study because of the time between when it was taken and our first observations (nearly 450 d), so we hoped to detect long-term variations with higher significance. Analysis of the newly added data confirmed that there is no significant variation of γ in time, which was already proposed in Paper II. When fitted for, the linear RV trends for both components were ~ 10 times smaller than their uncertainties. We can put a formal upper limit on the linear trend in γ at $0.8 \text{ m s}^{-1} \text{ d}^{-1}$. Notably, the RVs from the TRES spectrum matched the HIDES data very well, even without applying any zero-point shift (Fig. 8). The total time-span is now 1182 d with TRES, and 737 d without. The meaning of the RV variations of component B are discussed later.

In Table 3, we present updated orbital and physical parameters of KIC 10191056 A, under the assumption of constant γ , and utilizing new JKTEBOP results. Because the long-cadence LC shows shallower eclipses, the amount and time-span of the short-cadence data are sufficient (quarters Q02, Q04 and Q06–Q10) and there are no obvious spot-like modulation or pulsations present, thus the use of short-cadence data is preferable and justified. We adopted results of the fit to the complete short-cadence set, and this is the LC shown in Fig. 8.

With respect to Paper II, we have significantly reduced the errors in $K_{1,2}$ and dependent parameters (i.e. the relative mass uncertainties are now 0.8 and 1.1 per cent for the primary and secondary, respectively). The errors in radii are now slightly better as well (i.e. 1.2 and 1.6 per cent). In Table 8, we compare our current and previous results with those of Matson et al. (2017). We note a significant discrepancy in K_1 , which leads to disagreement in other parameters. This could be caused by the fact that Matson et al. (2017) used few observations in phases around eclipses, when the RV difference is small, and lines are blended.

Without the spectral analysis, we do not have independent T_{eff} and [M/H] estimates.

4.1.9 KIC 10583181

This system was observed 10 times with HIDES. However, we acquired only nine measurements of the faint secondary, so nine

spectra were used in TD. In the orbital fit with v2FIT, we took into account the presence of the circumbinary body reported by Borkovits et al. (2016). The circumbinary orbit was assumed to be Keplerian, and parametrized by period P_3 , eccentricity e_3 , moment of pericentre passage T_3 , longitude of pericentre ω_3 and semi-amplitude of modulation of the inner binary's systemic velocity K_3 . In such a mode, the parameter γ in v2FIT is defined as the systemic velocity of the whole triple system. Parameters of the outer orbit were found simultaneously with those of the inner binary.

The time-span of our HIDES observations is 482 d, while $P_3 = 1169.2$ d. Therefore, we could not set the outer period free in our fit (although we have data taken around the pericentre passage). We also fixed $e_3 = 0.06$ and $\omega_3 = 279^\circ$, which are values given by Borkovits et al. (2016),¹⁰ and we only searched for K_3 and T_3 . The resulting parameters of the inner orbit (only) are given in Table 3. Fig. 9 shows only the RV curves of the inner binary, while the modulation of γ induced by the third body is shown in Fig. 10.

Borkovits et al. (2016) do not give the value of amplitude of the ETVs, but list the $a \sin(i_3)$, from which we can estimate the expected scale of RV variation. From $a \sin(i_3) = 154.0(1) R_\odot$, and using P_3 and e_3 given above, we expect K_3 to be $6.674(7) \text{ km s}^{-1}$. Our orbital solution gives $7.2(1.6) \text{ km s}^{-1}$, in agreement with that expected. For the record, our value of $T_3 = 4494(53)$ d (JD 245 0000) is also in agreement with the value from Borkovits et al. (2016), 4503(6) d. Larger errors are, of course, the effect of poor time coverage of the outer orbit. The minimum companion mass, from our solution, is $0.66(14) M_\odot$.

Overall, our orbital solution is satisfactory, considering the relatively poor precision of the RVs. Our measurements are hampered by fast rotation (36 and 19 km s^{-1} for the primary and secondary, respectively) and the small contribution of the secondary to the total flux (~ 10 per cent). Yet, the rms of the fit for the primary is only 0.7 km s^{-1} . Relative mass uncertainties are also quite low (i.e. 2.3 and 1.7 per cent for the primary and secondary, respectively).

In Fig. 9, we also show the short-cadence *Kepler* LC, taken during quarters Q02, Q03 and Q7–Q10. Because of the presence of the third body, which strongly influences moments of eclipses, for the LC fit we used a similar approach as for KIC 7821010, and we analysed the data quarter-by-quarter. Additionally, we noted variations of the depth of minima, especially the flat (total) secondary. The lower panel of the LC fit in Fig. 9 shows residuals from single-quarter fits stacked together. A prominent feature is that the scatter during the secondary minimum is much lower than outside the eclipses. This suggests that the secondary, which turns out to be a solar-analogue, contains cool spots that evolve in time. There are also several flares recorded in the LC.

We also fitted for the contribution of the third light l_3/l_{tot} and we found it to be $0.12(2)$, i.e. larger than l_2 ($l_2/l_{\text{tot}} \simeq 0.084$), although probably variable (>0.12 in Q02, Q07, Q09 and Q10; <0.11 in Q03 and Q08). The variability might be a result of the satellite's positioning and rotation, as for KIC 3439031, but the total amount of l_3 is difficult to explain by contamination from nearby stars, so the bulk of it must come from the circumbinary companion. However, we do not see this companion in our spectra. Considering a relatively large minimum mass, this can be explained if the companion was a binary itself, composed of two M- or K-type stars, too faint to be detected with our approach. However, with our current data we cannot verify this.

¹⁰In v2FIT, ω_3 is defined for the outer body, while in Borkovits et al. (2016) it is defined for the inner binary. Thus, we added π (180°) in our fit.

The overall LC fit is quite good (rms $\simeq 1.7$ mmag), hampered mildly by the evolution of spots, and it led to relatively low uncertainties of radii (i.e. 0.7 and 1.0 per cent for the primary and secondary, respectively). We note that the primary is very similar, only slightly smaller, than the primary of KIC 10191056. The orbital periods and major semi-axes are also alike, both pairs accompanied by other bodies, and the main difference between them is, obviously, the secondaries. Moreover, the secondary in KIC 10583181 has almost identical mass as the secondary in KIC 8552540. It would be interesting to compare a number of such pairs (identical primaries with different secondaries, or vice versa) and to search for differences that could be caused by the influence of different companions (e.g. interaction of magnetic fields, influence of rotation on the internal structure and activity, etc.).

The ISPEC analysis was possible only for the primary. The influence of the third light was assumed to be constant across the spectrum, which is probably not entirely correct. However, given that we have no additional information about l_3 , this was the only reasonable assumption we could make. Depths of spectral lines were probably affected in a non-uniform way, so the results of this analysis should be treated with caution. We found that the system's chemical composition is probably similar to solar, and the primary is cooler than expected for the main sequence (MS). Our $T_{\text{eff},1} = 6730(140)$ K is, however, larger than 6425^{+260}_{-180} K from GDR2, although formally in 1σ agreement. We found no estimates of T_{eff} in the literature that would match values expected at the MS for this mass and solar metallicity. At the same time, the primary's radius R_1 is larger than predicted for the zero-age MS, which suggests it has evolved significantly. A more detailed discussion is presented in Section 4.2.

Without both effective temperatures, and information about the third light in bands other than *Kepler*'s, we are unable to estimate d_J . We estimate the distance on the basis of isochrone-calibrated absolute magnitudes M_{kep} in Section 4.2.

Finally, we compare our direct determination of absolute masses with the indirect approach from Devor et al. (2008). By comparing parameters obtained from analysing the TrES LC (T-Lyr-01013) and apparent magnitudes of the whole system with theoretical isochrones, Devor et al. obtained the most probable masses (and age) of the components: $1.749(19)$ and $1.049(15)$ M_{\odot} . The disagreement with absolute values from Table 3 is obvious but, surprisingly, the mass ratio agrees. This is another case (more are given in Paper II) that shows that, without any spectroscopic information, it is impossible to obtain reliable stellar parameters for eclipsing binaries.

4.1.10 KIC 10987439

This system has no new HIDES observations since Paper II, and only long-cadence *Kepler* photometry is available (Fig. 11), so we rely on our previous results. It is another case of a high-contrast pair (low flux ratio), for which the disentangled spectrum of the fainter component is not sufficient for reliable spectroscopic analysis ($S/N = 20$). It is, however, an important target, as we reached excellent precision in masses (0.34 and 0.32 per cent), and also very good precision in radii (i.e. 1.6 and 2.0 per cent for the primary and secondary, respectively). Please note that, as in KIC 4851217 or 10031808, the primary is actually the fainter star.

The ISPEC analysis of the TD spectrum of the secondary ($S/N = 134$) gave $T_{\text{eff},2} = 6490(90)$, the system's metallicity and α -enhancement indistinguishable from solar: $-0.03(5)$ and

$0.05(16)$ dex, respectively. The temperature is in excellent agreement with 6450^{+270}_{-25} K from GDR2. During the analysis, we assumed pseudo-synchronous rotation, because the predicted time-scale of synchronization (from JKTABSDIM) is only 93 Myr. Again, we could not use JKTABSDIM to calculate distance. We do it on the basis of isochrone-calibrated values in Section 4.2.

However, in addition to Paper II, in this work we run a Lomb-Scargle periodogram on the residuals of our fit. We detected a single, dominant peak at $\simeq 1.624$ d with two side lobes at $\Delta P \simeq \pm 0.0068$ d (or $\Delta\nu \simeq \pm 0.00258$ d $^{-1}$ in the frequency domain), and a variety of lower, but still very prominent peaks at periods between 2.5 and 4 d (Fig. 12). The amplitude of the dominant pulsation is only 33 ppm. We tentatively interpret this as γ Dor-type pulsations, originating most likely from the brighter, more massive secondary, but a detailed analysis is required. Comparison of our values of T_{eff} , $\log(g)$ and v_{mic} with distributions of those parameters in Kahraman Aliçavuş et al. (2016) tends to confirm our conclusion, although KIC 10987439 resides at the lower-mass edge of distributions. If pulsations are confirmed, then KIC 10987439 together with KIC 10031808 would double the number of precisely measured eclipsing binaries with γ Dor-type stars.

4.1.11 KIC 11922782

This system also has no new HIDES observations, and we kept the results of the analysis of the complete long-cadence LC (shown in Fig. 13) from Paper II. Short-cadence data are available only for pieces of Q02 and Q03. Similarly to KIC 8552540, the LC is affected by rapidly evolving spots, so two incomplete *Kepler* quarters of data would not be sufficient for proper fitting. Moreover, the depths and widths of the minima in the long-cadence curve has not been affected by longer exposure time.

The star is another case of a low flux ratio binary. For the record, the precision in masses (from Paper II) is $0.9 + 0.7$ per cent for the primary and secondary, respectively, and $3.8 + 7.4$ per cent analogously in radii. The uncertainty of the secondary's fractional radius r_2 is mainly affected by strong activity and rapid evolution (on a time-scale of days) of prominent, cool spots. Notably, the secondary is the lowest-mass star ($0.85 M_{\odot}$) in our entire *Kepler* sample of SB2s. However, the primary is an evolved and older analogue of the Sun, with a similar mass but significantly larger radius. The whole system is therefore interesting for several reasons.

Spectral analysis with ISPEC was possible only on the TD spectrum of the primary ($S/N = 149$). KIC 11922782 was found to be metal-poor with respect to the Sun, which was expected for an older system. Also, $T_{\text{eff},1} = 6000(110)$ K, which is higher than solar, can be explained by considering the metal depletion, although it disagrees with 5620^{+64}_{-70} K from GDR2. Rotationally broadened lines point strongly towards synchronous rotation, which, according to the theory, should be achieved after 20 Myr. The circular orbit is also not surprising, as the time-scale of circularization is only about 220 Myr. Lack of independent estimates of $T_{\text{eff},2}$ prevents us from using JKTABSDIM for distance calculations.

4.2 Age and evolutionary status

In Figs 14 and 15, we show a comparison of the results of our analyses with theoretical MESA isochrones. For each system, we determine the age at which the observed or calculated properties of both components are best represented. Because the stellar mass M is the most robust resulting parameter, which also strongly determines

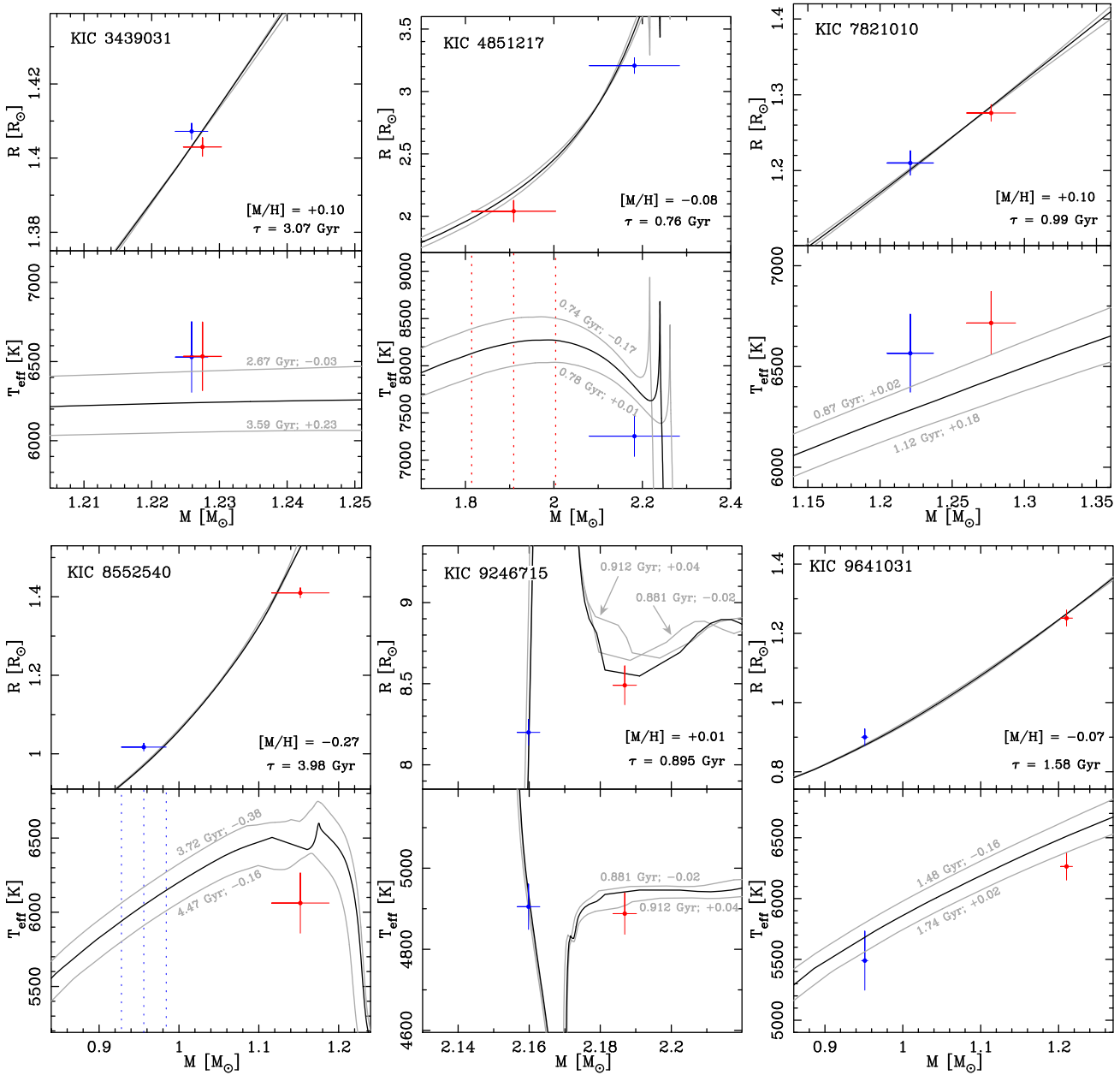


Figure 14. Comparison of our results with MESA isochrones on M/R (upper) and M/T_{eff} (lower) planes. Primaries are shown with red symbols, and secondaries with blue symbols, both with 1σ error bars. Black lines are isochrones for metallicities adopted from ISPEC analysis that best matches both components on both planes simultaneously, with $[M/H]$ and best-fitting age τ also labelled in black. When a T_{eff} has not been measured, dotted lines of a corresponding colour on the M/T_{eff} plane mark the mass and $\pm 1\sigma$ error of the component, in order to evaluate its T_{eff}^i . Grey lines represent isochrones for metallicity varied by $\pm 1\sigma$, that best match all available data on both planes. On M/R they are often undistinguishable from the black line, because of the age–metallicity degeneration. Their corresponding τ and $[M/H]$ are given on M/T_{eff} panels. This figure shows the results for KIC 3439031, KIC 4851217, KIC 7821010, KIC 8552540, KIC 9246715 and KIC 9641031.

the evolution of a star, we compare our data on mass/radius (M/R) and mass/effective temperature (M/T_{eff}) planes. The former is prone to age–metallicity degeneration, meaning the same M/R combination can be reproduced by various pairs of $[M/H]$ and τ . However, the M/T_{eff} plane is relatively insensitive to changes in τ , when a star is on the MS, but very sensitive to $[M/H]$. Therefore, a combination of M/R and M/T_{eff} planes can be used to determine the age and evolutionary status securely, as long as $[M/H]$ and at least one T_{eff} are estimated.

For systems with only one effective temperature determined with ISPEC, we use the best-fitting isochrone, and the dynamical mass estimate for the faint companion, to check the T_{eff} predicted for the given mass and metallicity at the given age. We use this isochrone-based T_{eff}^i together with the other T_{eff} as input in JKTABSDIM to evaluate the distance d_1 . This distance is then compared with a value from GDR2. In the case of KIC 10191056, both temperatures are estimated in such a way, and solar metallicity is assumed.

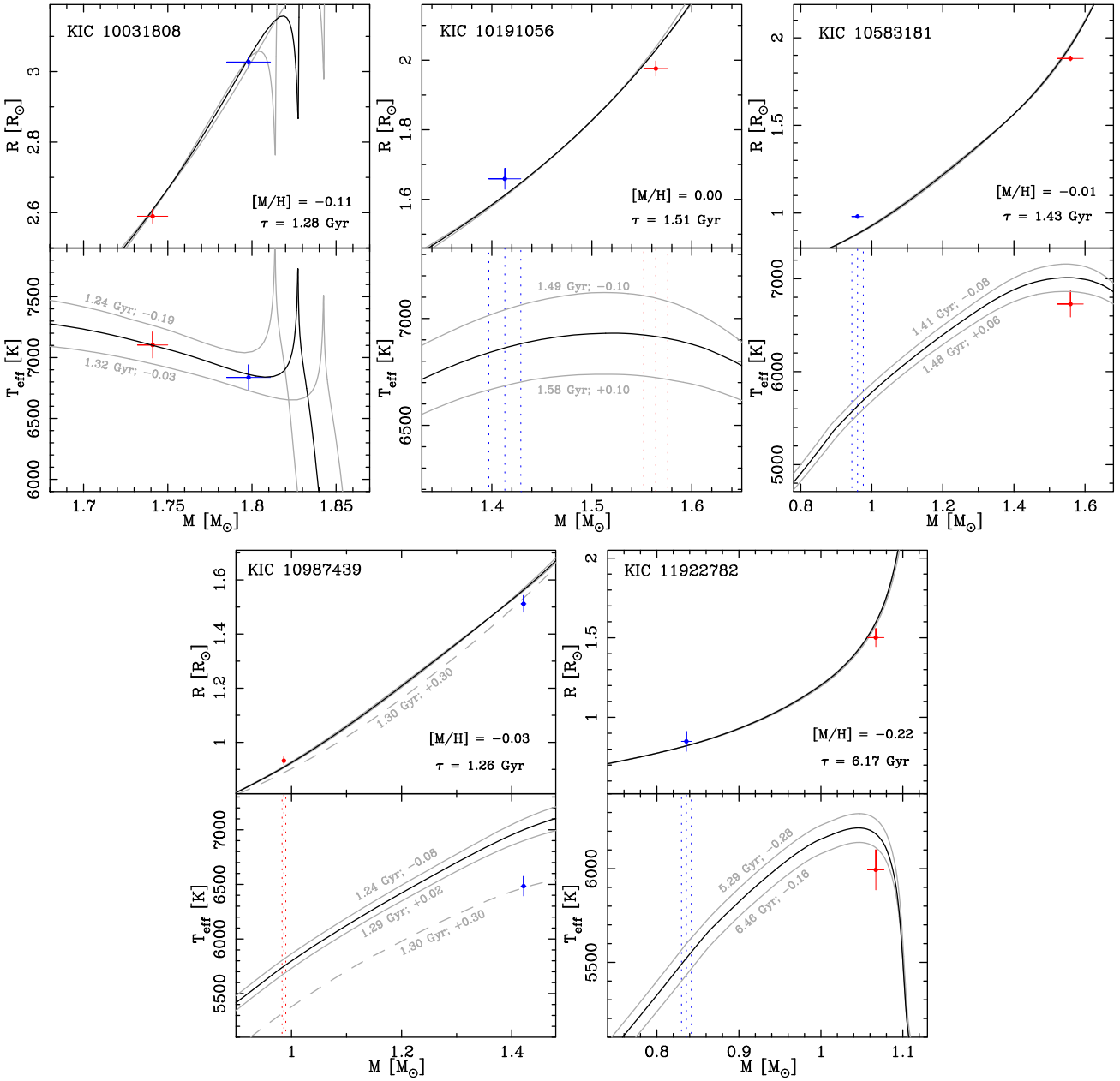


Figure 15. Same as Fig. 14 but for KIC 10031808, KIC 10191056, KIC 10583181, KIC 10987439 and KIC 11922782. For KIC 10191056, the $[M/H]$ and its uncertainty have been assumed. For KIC 10987439, we additionally plot an $\tau = 1.3 \text{ Gyr}$, $[M/H] = +0.30 \text{ dex}$ isochrone (dashed line). See text for details.

4.2.1 KIC 3439031

This is a system with two nearly identical stars residing on the MS, but evolved with respect to the zero-age main sequence (ZAMS). The age of 3.07 Gyr is, as expected, below the upper limit for orbit circularization (i.e. 4.27 Gyr). The agreement of the model with temperatures is quite good, but mainly due to relatively large errors in T_{eff} and $[M/H]$. Notably, individual values of $[M/H]$ and $[\alpha/\text{Fe}]$ from ISPEC were almost identical: $[M/H] = 0.09(13)$ and $0.10(13)$ dex for the primary and secondary, respectively, and $[\alpha/\text{Fe}] = 0.02(14)$ and $0.03(14)$ dex, analogously. At the same time, the temperatures we adopted led to d_j that agrees very well with GDR2. Therefore, we suspect that it is the metallicity scale that is systematically shifted off, rather than the temperatures. Even

so, the age will still be $> 2.5 \text{ Gyr}$, and the conclusions about the evolutionary status remain unchanged.

4.2.2 KIC 4851217

Only one estimate of T_{eff} from spectra is available for this pair. We estimated the age of this system to be 760 Myr, and we conclude that the more massive secondary has nearly finished its MS evolution. From the M/R diagram only, this system would be younger, but then the temperature of the secondary would be significantly larger. This component is now at the stage when T_{eff} changes rapidly, in comparison to earlier MS stages, so its age determination is highly sensitive to the temperature. The best-fitting isochrone, for $[M/H]$

found in ISPEC, matches our parameters at $<3\sigma$ level. A slightly better match is found for higher metallicities, so we suspect that this system is more metal abundant than we have found. It is worth noting that the secondary is a fast rotator, which might have affected our analysis, but in any case its evolutionary stage is established securely.

The isochrone-predicted effective temperature T_{eff}^i of the fainter but hotter primary is 8250(300) K (uncertainty includes error in [M/H]; see Fig. 14). When used in JKTABSDIM together with $T_{\text{eff},2}$ from ISPEC, the predicted distance d_1 is 1090(70) pc, assuming $E(B - V) = 0.03$ mag to reach consistency between all bands. The agreement with 1195(53) pc from GDR2 is therefore quite good. This shows that, although we do not have complete information about KIC 4851217, our results are reliable.

4.2.3 KIC 7821010

This pair consists of two MS components, and thus the strongest age constraints (for a particular value of [M/H]) come from the M/R diagram, while the M/T_{eff} plane helps us to assess the metal content. Assuming the ISPEC value of $[\text{M}/\text{H}] = +0.10$ dex, we obtain the best overall fit for $\tau = 0.99$ Gyr, with the model matching our results on the mass–radius plane very well, and within 2σ on the M/T_{eff} diagram. A better match ($\sim 1\sigma$) is obtained for lower $[\text{M}/\text{H}] = +0.02$ dex (-1σ from the ISPEC value), for which the best overall fit is found for $\tau = 0.87$ Gyr. We can therefore confidently conclude that KIC 7821010 is younger than the Sun, so the small metal enhancement is not surprising. Notably, the secondary is similar in mass to both components of KIC 3439031, but is significantly smaller (and likely hotter). Also, both systems have similar metallicities. All this is consistent with KIC 7821010 being younger than KIC 3439031 ($\tau \simeq 3.1$ Gyr).

4.2.4 KIC 8552540 (V2277 Cyg)

The primary of KIC 8552540 comes to the end of its MS evolution, which is supported by its oversized radius and lower temperature. The best-fitting isochrone, assuming the ISPEC value of $[\text{M}/\text{H}] = -0.27$ dex, is found for $\tau \simeq 4.0$ Gyr. Varying the metallicity by its 1σ uncertainty changes τ by 0.3–0.5 Gyr. The ‘older’ value, for the higher metal content of -0.16 dex, seems to better match $T_{\text{eff},1}$, but still the agreement between our temperature determination from ISPEC and the prediction for $[\text{M}/\text{H}] = -0.27$ dex is formally within 2σ . As in the case of KIC 4851217, the component analysed with ISPEC rotates rapidly (~ 67 km s $^{-1}$), which might have affected the results of spectral analysis.

The formally best-fitting 3.98 Gyr, -0.27 dex isochrone predicts the temperature of the fainter secondary to be $T_{\text{eff},2}^i = 6050(230)$ K, which is almost exactly the same as $T_{\text{eff},1}$. This clearly contradicts the fact that the *Kepler* LC shows two very much uneven eclipses (Fig. 4), which (for $e = 0$) means different surface brightnesses, and hence temperatures. Even though a formal agreement with isochrones exists, our temperature and/or metallicity scales are likely affected, presumably by the rotation, as already mentioned. Notably, a solar-composition model can reproduce our $T_{\text{eff},1}$ and the M/R diagram quite well for $\tau = 5$ Gyr.

For the distance estimates with JKTABSDIM, we used several pairs of isochrone-predicted temperatures, taken from isochrones ranging from $[\text{M}/\text{H}] = 0.0$ dex (5 Gyr) to -0.38 dex (3.72 Gyr). All the resulting distances are significantly above the value of 231(1) pc from GDR2: that is, 269 pc for $[\text{M}/\text{H}] = -0.38$ dex, $T_{\text{eff},1}^i = 6630$ K, $T_{\text{eff},2}^i = 6180$ K, $E(B - V) = 0.09$ mag; 267 pc for -0.27 dex,

6440 K, 6050 K, 0.06 mag; 266 pc for -0.16 dex, 6360 K, 5910 K, 0.03 mag; and 259 pc for 0.0 dex, 6060 K, 5700 K, and 0.0 mag. In all cases, we assumed 200 K errors in temperatures, we obtained ~ 9 pc uncertainty in distance and the $E(B - V)$ value was found by forcing individual distances from the V, I, J, H and K bands to give the lowest spread.¹¹

We could not obtain an ISPEC fit with the assumed $[\text{M}/\text{H}]$ higher than our result from Table 3. Nevertheless, we conclude that KIC 8552540 is probably more metal abundant and its components hotter than we have found. Additional problems with more reliable age and $[\text{M}/\text{H}]$ assessment come from the fact that the precision in masses is relatively poor, which prevents us from using other information (i.e. flux ratio, absolute magnitudes from GDR2 distance) to discriminate between various $[\text{M}/\text{H}] - \tau - T_{\text{eff}}$ scenarios. Nevertheless, our results are good enough to conclude that both components are still at the MS (with the primary approaching its end), and the system is a few Gyr old.

4.2.5 KIC 9246715

The exact evolutionary stage of KIC 9246715 was uncertain. Rawls et al. (2016) established from asteroseismology that the oscillating star is at the core-He burning phase (secondary red clump). In their comparison with MESA models, they assumed a higher than typical mixing-length parameter $\alpha = 2.5$, in order to explain the fact that the primary’s radius is smaller than normally expected from a horizontal-branch star. Because, in their solution, both components are very similar to each other, they concluded that both stars are currently on the red clump, although they also considered an option where both components are still on the red giant branch (RGB; before core-He burning), but would have to be of a slightly different age.

Our solution shows that the two masses differ significantly ($>6\sigma$), and the primary’s radius is also slightly larger than that obtained by Rawls et al. (Table 6). Large enough, in fact, that the secondary can be a horizontal-branch star, without assuming an abnormal mixing-length parameter, or weaker convective overshooting (which was also discussed by Rawls et al. 2016). We found a very good match on both M/R and M/T_{eff} planes for an age of nearly 0.9 Gyr (Fig. 14). In such a situation, the primary is just after He ignition in the core ($M > 2.18 M_{\odot}$), while the secondary is still on the RGB phase, growing rapidly. As this phase is very short, the secondary constrains the age to a precision of only a few Myr. An age–metallicity degeneration is still present, but our $[\text{M}/\text{H}]$ estimates allow us to reduce the overall uncertainty in τ (for this particular set of models) to <20 Myr.

4.2.6 KIC 9641031 (FL Lyr)

The notable differences between our recent solution and the one from Popper et al. (1986) are smaller R_2 , lower $[\text{M}/\text{H}]$ and larger T_{eff} (Table 7), all of which results in a much better match to the isochrones than previously. As can be seen in Fig. 14, both components are well represented by a 1.58 Gyr, $[\text{M}/\text{H}] = -0.07$ dex model on the M/R plane, as well as on the M/T_{eff} plane when $[\text{M}/\text{H}]$ uncertainty is taken into account. The agreement on the M/R diagram would not be possible with the parameters of Popper et al., and their very high metal content (+0.32 dex) was assumed

¹¹In this case, we used I instead of B , because it was available in Simbad, and the B -band magnitude was giving distances that very much deviated from the other bands.

to match the effective temperatures, which themselves were derived from now-outdated calibrations, and were indirectly dependent on the flux and radius ratio in their solution. We claim that our results in this work are more credible.

Notably, FL Lyr is listed in the DEBCat,¹² which is a collection of the best-studied DEBs (Southworth 2015). Even very recently, it has been used for creating state-of-the-art calibrations of fundamental stellar parameters (e.g. Eker et al. 2015; Graczyk et al. 2017). However, this case shows that many systems studied several decades ago may have been re-evaluated and their parameters need to be updated with better precision and accuracy, if they are to be used for the purposes of modern astrophysics.

4.2.7 KIC 10031808

A comparison of our results with the MESA isochrones shows an excellent match on both M/R and M/T_{eff} diagrams for the age of 1.28 Gyr. The overall uncertainty in τ is well below 100 Myr (taking into account errors in all parameters), which makes the estimate of the age of this system especially important for asteroseismology. KIC 10031808 is one of very few examples of a well-studied eclipsing binary with a γ Dor pulsator, which, in this case, we suspect is the hotter, less massive primary. The cooler secondary could also have been a pulsator in the past, but currently it might be too evolved for stable pulsation modes. Considering that the two masses do not differ very much, it is interesting to see a system in which both components are close to the end of their MS lifetimes, but (probably) only one is still showing pulsations. With a complete set of high-precision and high-accuracy stellar parameters, and a good age estimate, KIC 10031808 should be a subject of a dedicated, detailed asteroseismic study, which we strongly encourage.

4.2.8 KIC 10191056 A

In this case, where we have no independent estimates of effective temperatures, we decided to repeat the approach from Paper II, and fit a solar-composition ($[\text{M}/\text{H}] = 0.0$) isochrone to the M/R only, but using the updated parameters and MESA models. We also assumed 0.1 dex as the 1σ uncertainty in $[\text{M}/\text{H}]$ to estimate the variations in age and the temperatures.

The best fit, within $\sim 1\sigma$ agreement, was found for $\tau = 1.51$ Gyr. The primary's radius suggests a significant deviation from the ZAMS. The predicted values of T_{eff}^i are nearly identical: 6880(200) and 6850(180) K for the primary and secondary, respectively. This is consistent with the LC showing nearly equal-depth eclipses. To estimate the distance, we followed the same procedure as in Paper II, where we only used apparent V - and I -band magnitudes, corrected for the third light: 11.19(17) and 10.51(5) mag, respectively. These values come from fitting the V - and I -band LCs, obtained from ASAS-K (see Paper II). The GDR2 distance of 613(8) pc is reached when $E(B - V)$ is assumed to be 0.081 mag. In such a case, the two individual distances are 650(70) and 608(26) for the V and I band, respectively, and their weighted average is 613(31) pc. The isochrone-predicted flux ratio in the *Kepler* band is 0.61(17), which agrees within errors with 0.68(4) from the LC fit.

We can also estimate the isochrone-predicted mass of the tertiary component KIC 10191056 B. For the l_2/l_1 value predicted by isochrones, the l_3/l_{tot} contribution of 0.160(9) is reproduced by a

star of $M_B = 1.23(3) M_{\odot}$. The GDR2 lists GP magnitudes of both A and B. The assumed isochrone predicts that the total absolute GP magnitude of A is 1.73(12) mag, and the magnitude difference from GDR2 is 1.923(6) mag. Thus, the absolute GP magnitude of B would be 3.65(12) mag. This value is reproduced by a star of $M_B = 1.230(25) M_{\odot}$, which is the same as the previous value. This consistency suggests that the component B is an F-type star, gravitationally bound to the eclipsing pair A.

4.2.9 KIC 10583181

In this system, both the primary and secondary are much larger than expected at the ZAMS. While this can be easily explained by evolution for the primary, the reason why the secondary is oversized must be different. Most likely, it is related to activity and fast rotation. This is not surprising, as a similar or even a higher level of inflation is observed in other short-period systems with components of nearly solar mass, such as for the primary of HP Aur ($P = 1.42$ d, $M = 0.954 M_{\odot}$, $R = 1.028 R_{\odot}$; Lacy et al. 2014), the secondary of ZZ UMa ($P = 2.30$ d, $M = 0.972 M_{\odot}$, $R = 1.16 R_{\odot}$; Lacy & Sabby 1999) and the secondary of KIC 8552540 ($P = 1.06$ d, $M = 0.956 M_{\odot}$, $R = 1.02 R_{\odot}$; Table 3). However, the secondary of KIC 9641031 ($P = 2.18$ d, $M = 0.951 M_{\odot}$, $R = 0.900 R_{\odot}$; Table 3) does not show such behaviour. The exact reason for the radius discrepancy of KIC 10583181 B is unclear to us.

We could not find a satisfactory fit to both components simultaneously, so we decided to search for the age of the system based on the primary only. An isochrone for $\tau = 1.43$ Gyr nicely reproduces its position on the M/R plane, and is in decent agreement with our T_{eff} estimates. As expected, it predicts the primary to be near the end of the MS stage. The match is better when the $[\text{M}/\text{H}]$ error is taken into account, which resembles the situation with KIC 4851217 and KIC 8552540. In all these cases, the possible factor affecting the ISPEC analysis is probably the rotational velocity. Nevertheless, the agreement is still acceptable, and the evolutionary stage is determined securely.

The adopted best-fitting isochrone predicts the secondary to have $T_{\text{eff}}^i = 5630(160)$ K. Unfortunately, because this system is a triple with significant flux contribution from the third body, and we have no information on l_3 in bands other than *Kepler*'s, we cannot use JKTABSDIM to estimate the distance. Instead, we calculate the apparent magnitude of the primary, and compare it to the absolute one, predicted by MESA isochrones. As stated above, we suspect l_3 was varying slightly throughout the *Kepler* observations. Therefore, for the following analysis, we take its conservative uncertainty, and assume its contribution to be 0.12(2).

With the primary's contribution to the total flux of 0.796(20), its apparent magnitude should be 11.26(3) mag.¹³ The absolute brightness, estimated from the isochrone, is 2.28(20) mag, with uncertainty in $[\text{M}/\text{H}]$ and mass taken into account. Analogously, for the secondary, we obtain the apparent magnitude of 13.70(4) mag, and absolute brightness of 4.95(18) mag. The weighted average of the distance module is therefore 8.85(19) mag, which translates into a distance (without extinction) of 589(52) pc. To level it with the GDR2 value of 445(5) pc, we need to assume $E(B - V) \simeq 0.20$ mag. This would require the equivalent width of the sodium D1 line to be around 0.4 Å, but in the spectra we measured it to be only

¹²<http://www.astro.keele.ac.uk/~jkt/debcat/>

¹³We do not take into account the uncertainty of the satellite's photometric zero-point, but we understand it might introduce an additional source of error.

0.192(16) Å, that is, $E(B - V) < 0.1$ mag (Munari & Zwitter 1997). We would also like to note that the isochrone-predicted flux ratio l_2/l_1 of 0.086(30) agrees with the value of 0.105(3) from the LC fit.

We do not attempt to estimate the mass of the tertiary from isochrones, as this object might be a binary itself, and its true contribution to the total flux in the *Kepler* band is actually uncertain.

A better insight into this system would be possible with additional information about the secondary and tertiary. The former can come from analysis of a higher S/N disentangled spectrum, which requires additional observations with a telescope larger than OAO-188cm, and/or advanced post-processing. The latter can be achieved with multicolour photometry, even from the ground. Observations with ~ 2 mmag precision are certainly possible, and the flat secondary eclipse helps to constrain the fluxes in the LC analysis.

4.2.10 KIC 10987439

With masses and radii measured to a very high precision, this system poses a challenge to isochrone fitting. A good fit (within 2σ) is achieved on the M/R plane to both components with an isochrone of $\tau = 1.26$ Gyr. The more massive secondary, which dominates the total flux of the system, does not seem to be very evolved, and the primary is not significantly inflated (similarly to KIC 9641031 B). Unfortunately, the ISPEC value of $T_{\text{eff},2}$ is significantly (~ 500 K) lower than 7000(110) K, which the isochrone predicts. This cannot be explained by the rotation $v \sin(i) = 7.16$ km s $^{-1}$, or by the S/N of the disentangled spectrum (~ 135). All the ISPEC runs, for which the starting T_{eff} was set to 7000 K or much higher, converged to values around 6500 K. Also, when the initial [M/H] was set to higher values (~ 0.2 –0.3 dex), the result was the same. In an additional check, we used four line depth ratio versus T_{eff} calibrations from Kovtyukh, Soubiran & Belik (2004) that utilize lines in the available wavelength regions and have the smallest rms (below 50 K). In this way, we obtained the average $T_{\text{eff}}^L = 6380(100)$ K, supporting the ISPEC result. This discrepancy between models and ISPEC is puzzling. However, we believe that the key is the metallicity scale, which might have been affected because of the shortest wavelength range, on which the analysis was performed. The blue end of the TD spectrum is at 5470 Å, while in case of other stars it is at 5030 Å (except for KIC 7821010).

We find a very good match to the $T_{\text{eff},2}$ value on the MS for [M/H] = +0.30 dex isochrones. The formally best fit was found for the age of ~ 1.3 Gyr. We plot this model in Fig. 15 as well, for comparison. The flux ratios l_2/l_1 predicted by the isochrones are 7.00(25) and 6.37(77) for [M/H] = +0.30 and -0.03 dex, respectively. While the latter is much closer to the value of 6.5(1.1) obtained from LC fit, both are in formal agreement within error bars.

The effective temperatures predicted by the [M/H] = -0.03 dex, $\tau = 1.26$ Gyr isochrone are $T_{\text{eff},1} = 5750(80)$ K and $T_{\text{eff},2} = 7000(110)$ K. The distance obtained with JKTABSDIM for these values is 339(11) pc, under the assumption of $E(B - V) = 0.1$ mag, made to reach the consistency between various bands. When the ISPEC value of $T_{\text{eff},2}$ is used, the distance is 333(13) pc with $E(B - V) = 0.0$ mag. Finally, $T_{\text{eff},1}^i$ predicted by the [M/H] = +0.30 dex, $\tau = 1.30$ Gyr isochrone is 5330(80) K. Together with $T_{\text{eff},2}$ from ISPEC, it leads to the distance of 326(11) pc at $E(B - V) = 0.1$ mag. We measured the equivalent width of the interstellar sodium D1

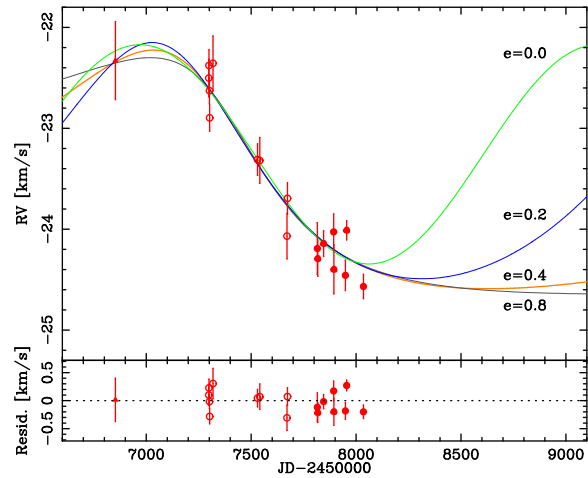


Figure 16. RV measurements of KIC 10191056 B, and examples of orbital solutions for selected eccentricities (labelled). Old HIDES, new HIDES and TRES data are plotted with open circles, filled circles and a triangle, respectively. The lower panel shows residuals for $e = 0.8$, but other solutions give residuals that are practically indistinguishable.

line and found it to be 0.16(1) Å. According to calibrations by Munari & Zwitter (1997), this corresponds to $E(B - V) \sim 0.05$ mag. This favours the cases with the $T_{\text{eff},2}$ from ISPEC. All values are significantly lower than 374(4) pc from GDR2. In any case, both components of KIC 10987439 are currently at the MS, and the age of the systems seems to be ~ 1.3 Gyr. With the γ Dor-type pulsations detected from the dominant (secondary) star, which has its parameters well constrained, KIC 10987439 is worth further detailed studies. It offers an interesting insight into the mechanisms of pulsations and their stability conditions, especially considering that the pulsator seems to reside at the low-mass edge of the γ Dor instability strip.

4.2.11 KIC 11922782

This system shows one of the lowest metallicities, and is also the oldest. The best-fitting [M/H] = -0.22 dex isochrone was found for $\tau = 6.17$ Gyr. The primary, which is similar in mass to the Sun, but much larger, is currently at the end of its MS life. Notably, the 6.17 Gyr isochrone matches both components on the M/R plane very well, which is not always observed in stars of mass similar to the secondary. The agreement with measured $T_{\text{eff},1}$ is also quite good, within 2σ , and even better when the [M/H] error is taken into account. In terms of masses and metallicity, KIC 11922782 is

Table 9. New HIDES RV measurements of KIC 10191056 B.

BJD 245 0000	v (km s $^{-1}$)	ε (km s $^{-1}$)	t_{exp} (s)	S/N
6852.954108 ^a	-22.329	0.387	480	16
7815.288473	-24.192	0.257	1500	31
7817.272376	-24.292	0.175	1500	48
7845.230234	-24.143	0.127	1500	29
7893.090781	-24.027	0.178	1500	30
7894.155920	-24.399	0.242	1800	25
7949.014405	-24.458	0.151	1630	45
7955.090230	-24.011	0.096	1511	50
8035.000297	-24.568	0.121	1588	46

^aFrom the TRES spectrum from 2014.07.14.

Table 10. Parameters of orbital solutions to the RVs of KIC 10191056 B for different (fixed) eccentricities, and mass of the host $M_B = 1.23(3) M_\odot$. Uncertainties are formal fit errors. The rms of a fit varies from 196 m s^{-1} for $e = 0.0$ to 189 m s^{-1} for $e = 0.8$.

e (fix)	P (d)	K (km s^{-1})	$a \sin(i)$ (au)	$f(m)$ (M_J)	$m \sin(i)$ (M_J)
0.0	2180 ± 380	1.087 ± 0.140	0.22 ± 0.01	0.30 ± 0.05	80 ± 11
0.1	2350 ± 1320	1.116 ± 0.328	0.25 ± 0.06	0.35 ± 0.20	83 ± 30
0.2	2800 ± 1990	1.171 ± 0.436	0.28 ± 0.13	0.46 ± 0.33	91 ± 40
0.3	3680 ± 1450	1.187 ± 0.514	0.35 ± 0.06	0.58 ± 0.24	99 ± 45
0.4	4920 ± 1330	1.183 ± 0.535	0.41 ± 0.05	0.70 ± 0.21	104 ± 48
0.5	6750 ± 1720	1.177 ± 0.539	0.47 ± 0.05	0.78 ± 0.24	109 ± 51
0.6	9760 ± 2640	1.174 ± 0.539	0.54 ± 0.06	0.88 ± 0.29	113 ± 53
0.7	$15\,500 \pm 4530$	1.172 ± 0.538	0.61 ± 0.07	0.99 ± 0.35	118 ± 57
0.8	$29\,280 \pm 9130$	1.172 ± 0.538	0.68 ± 0.09	1.10 ± 0.44	122 ± 58

similar to V636 Cen ($1.052 + 0.854 M_\odot$, -0.20 dex; Clausen et al. 2009). Also, the radii of secondaries are comparable: $0.830 R_\odot$ in V636 Cen versus $0.849 R_\odot$ in this work. The age found for V636 Cen is ~ 1.4 Gyr, assuming different mixing length scales for the two components. The much larger radius of the primary in KIC 11922782 ($1.501 R_\odot$ versus $1.018 R_\odot$ in V636 Cen) confirms the older age. Additionally, we did not have to fine tune the mixing length parameters to reach agreement with models.

The best-fitting isochrone predicts $T_{\text{eff},2}^i = 5520(120)$ K. When used in JKTABSDIM for distance determination, this results in $d_J = 227(12)$ pc, under the assumption of $E(B - V) = 0.09$ mag. This is in good agreement with $236(2)$ pc from GDR2.

4.3 KIC 10191056 Bb – a candidate M dwarf

In Paper II, we presented two hypotheses about the origin of the RV variations of KIC 10191056 B: (i) we observe motion on the orbit around a common centre of mass with the eclipsing pair A; (ii) we see a short-period (10–20 d) modulation induced by a massive planet or low-mass brown dwarf. The new HIDES observations, supported with the TRES spectrum from 2014 July, make the former very unlikely, and rule out the latter. New observations do not match any of the previously proposed solutions. However, the motion of B is very clear.

In Fig. 16, we show all the RV measurements for KIC 10191056 B. The new measurements are presented in Table 9. New HIDES data (after JD = 245 7800) cluster at lower values, while the TRES point is at a similar level as the earliest ones from HIDES (no zero-point shift was assumed; see Section 4.1.8). We clearly see a gradual drop in velocity, with some curvature. Because we do not see a significant long-term upwards trend in γ of the pair A, this observed RV drop must be caused by another body in the system (Bb), which is orbiting B with a period much longer than the time-span of our observations.

With only a fraction of the orbit covered, we cannot fit for P and e simultaneously. Instead, we run a number of fits with fixed eccentricity that varied from 0.0 to 0.8. Their results are shown in Table 10. Solutions with $e > 0.8$ led to very long orbital period and showed problems with convergence, so we decided not to present them. Nevertheless, such high eccentricities are not impossible. The circular ($e = 0$) solution sets the lower limit on the period of Bb at $2180(380)$ d. All solutions have similar quality, with $\text{rms} \simeq 190 \text{ m s}^{-1}$.

Independently of the assumed e , all solutions lead to RV amplitude of $\sim 1.1 \text{ km s}^{-1}$, which strongly constrains the minimum mass of the companion. We obtained $m \sin(i)$ between 80 and 122

Jupiter mass (M_J), with large uncertainties coming mainly from the unknown P , and assuming a theoretically predicted mass of the host $1.23(3) M_\odot$. This means that the companion is most likely a late-M type star or, rather unlikely, a massive brown dwarf. More observations are needed to set further limits on orbital parameters and $m \sin(i)$. Even a few observations taken throughout 2019 will allow us to distinguish between low- and high-eccentricity solutions. The spectra need to be of a sufficiently high resolution, and taken around quadratures of the pair A, to have the narrow lines of B distinguishable and well separated from the broad lines of the pair A. Unfortunately, the available observations from LAMOST (e.g. Frasca et al. 2016; Zong et al. 2018), or those used by Matson et al. (2017), do not have sufficient spectral resolution. A better estimate of M_B would also be welcome.

5 CONCLUSIONS

We have presented updated results for 11 (three new) DEBs from the original observing field of the *Kepler* satellite, based on new observations, refined LC fits and/or additional complementary methods of analysis. We improve our knowledge of the systems, mainly by adding new information, crucial for assessing the age and evolutionary status of the studied targets. In this work, we have studied a variety of interesting systems, including a double-giant pair with one of the components at the core-He burning phase, a probable quadruple, various pairs with components at vastly different phases of MS evolution, three DEBs with pulsating (δ Sct and γ Dor) components, a pair of twins, and a pair with a low-mass ($0.85 M_\odot$) secondary. A significant number of systems have their physical absolute parameters derived with < 2 per cent uncertainties. For two targets, KIC 9246715 and KIC 9641031 (FL Lyr), our updated results are in better agreement with evolutionary models than in the previous studies. There are still open questions and things to improve in some cases. First, the LCs could be cleaned from the influence of spots or pulsations, and a more careful detrending could be performed. The effective temperatures of fainter components could be derived, but this requires more spectroscopic observations and higher S/N spectra. We also encourage the community to study the pulsations in the presented systems.

ACKNOWLEDGEMENTS

We would like to thank the following: Sergi Blanco-Cuaresma from the Harvard-Smithsonian Center for Astrophysics, the creator of ISPEC, for making available the version of his code before it was made public; the organisers and presenters of the 2018

iSpec Spectroscopic Summer School in Wrocław, especially Ewa Niemczura (Astronomical Institute, University of Wrocław), Barry Smalley (Keele University Astrophysics Group) and Sergi Blanco-Cuaresma, for fruitful discussions, tips, suggestions and comments regarding the spectral analysis; and Miroslav Fedurco from the Pavol Josef Šafárik University in Košice, Slovakia, for discussing the results.

This research has made use of the SIMBAD data base, operated at CDS, Strasbourg, France. This work has made use of data from the European Space Agency (ESA) mission *Gaia* (<http://www.cosmos.esa.int/gaia>), processed by the *Gaia* Data Processing and Analysis Consortium (DPAC; <http://www.cosmos.esa.int/web/gaia/dpac/consortium>). Funding for the DPAC has been provided by national institutions, in particular the institutions participating in the *Gaia* Multilateral Agreement.

KGH, MR and AP acknowledge support provided by the Polish National Science Center through grants no. 2016/21/B/ST9/01613, 2015/16/S/ST9/00461 and 2016/21/B/ST9/01126, respectively. This work was partially supported by the Japan Society for the Promotion of Science (JSPS) KAKENHI Grant Number 16H01106.

REFERENCES

- Allende Prieto C. et al., 2008, *Astron. Nachr.*, 329, 1018
 Alonso R. et al., 2004, *ApJ*, 613, L153
 Asplund M., Grevesse N., Sauval A. J., Scott P., 2009, *ARA&A*, 47, 481
 Bagnuolo W. G., Jr, Gies D. R., 1991, *ApJ*, 376, 266
 Blanco-Cuaresma S., Soubiran C., Heiter U., Jofré P., 2014, *A&A*, 569, A111
 Blanco-Cuaresma S. et al., 2016, in 19th Cambridge Workshop on Cool Stars, Stellar Systems, and the Sun (CS19). Zenodo, p. 22
 Borkovits T., Hajdu T., Szakács J., Rappaport S., Levine A., Bíró I. B., 2016, *MNRAS*, 455, 4136
 Bright J. C., Torres G., 2017, *ApJ*, 850, 10
 Brogaard K. et al., 2018, *MNRAS*, 476, 3729
 Brown A. G. A. et al. (Gaia Collaboration), 2018, *A&A*, 616, A1
 Choi J., Dotter A., Conroy C., Cantiello M., Paxton B., Johnson B. D., 2016, *ApJ*, 823, 102
 Clausen J. V., Bruntt H., Claret A., Larsen A., Andersen J., Nordström B., Giménez A., 2009, *A&A*, 502, 253
 Coelho P., Barbay B., Meléndez J., Schiavon R. P., Castilho B. V., 2005, *A&A*, 443, 735
 Conroy K. E., Prša A., Stassun K. G., Orosz J. A., Fabrycky D. C., Welsh W. F., 2014, *AJ*, 147, 45
 Debosscher J. et al., 2013, *A&A*, 556, A56
 Devor J., Charbonneau D., O'Donovan F. T., Mandushev G., Torres G., 2008, *AJ*, 135, 850
 Dotter A., 2016, *ApJS*, 222, 8
 Eker Z. et al., 2015, *AJ*, 149, 131
 Frasca A. et al., 2016, *A&A*, 594, A39
 Gaulme P. et al., 2016, *ApJ*, 832, 121
 Gies D. R., Williams S. J., Matson R. A., Guo Z., Thomas S. M., Orosz J. A., Peters G. J., 2012, *ApJ*, 143, 137
 Gies D. R., Matson R. A., Guo Z., Lester K. V., Orosz J. A., Peters G. J., 2015, *ApJ*, 150, 178
 Gilmore G. et al., 2012, *Msngr.*, 147, 25
 Graczyk D. et al., 2017, *ApJ*, 837, 7
 Gray R. O., Corbally C. J., 1994, *AJ*, 107, 742
 Grevesse N., Asplund M., Sauval A. J., 2007, *Space Sci. Rev.*, 130, 105
 Gustafsson B., Edvardsson B., Eriksson K., Jørgensen U. G., Nordlund Å., Plez B., 2008, *A&A*, 486, 951
 Hartman J. D., Bakos J., Stanek K. Z., Noyes R. W., 2004, *ApJ*, 128, 1761
 Helminiak K. G. et al., 2012, *MNRAS*, 425, 1245
 Helminiak K. G., Ukita N., Kambe E., Konacki M., 2015a, *ApJ*, 813, L25(K924)
 Helminiak K. G. et al., 2015b, *MNRAS*, 448, 1945
 Helminiak K. G., Ukita N., Kambe E., Kozłowski S. K., Sybilska P., Ratajczak M., Maehara H., Konacki M., 2016, *MNRAS*, 461, 2896(Paper I)
 Helminiak K. G. et al., 2017a, *MNRAS*, 468, 1726(Paper II)
 Helminiak K. G., Ukita N., Kambe E., Kozłowski S. K., Pawłaszek R., Maehara H., Baranec C., Konacki M., 2017b, *A&A*, 602, A30
 Izumiura H., 1999, in Chen P. S., ed., Proc. 4th East Asian Meeting on Astronomy. Chinese Academy of Sciences, Yunnan Observatory, p. 77
 Kahraman Aliçavuş F. et al., 2016, *MNRAS*, 458, 2307
 Kambe E. et al., 2013, *PASJ*, 65, 15
 Kepler Mission Team, 2009, VizieR Online Data Catalog, 5133
 Kervella P., Thévenin F., Di Folco E., Ségransan D., 2004, *A&A*, 426, 297
 Kirk B. et al., 2016, *AJ*, 151, 68
 Konacki M., Mutterspaugh M. W., Kulkarni S. R., Helminiak K. G., 2010, *ApJ*, 719, 1293
 Kovtyukh V. V., Soubiran C., Belik S. I., 2004, *A&A*, 427, 933
 Kurucz R. L., 1992, in Barbuy B., Renzini A., eds, Proc. IAU Symp. 149, The Stellar Population of Galaxies. Kluwer Academic, Dordrecht, p. 225
 Lacy C. H. S., Sabby J. A., 1999, *IBVS*, 4755, 1
 Lacy C. H. S., Torres G., Wolf M., Burks C. L., 2014, *AJ*, 147, 1
 Lastennet E., Valls-Gabaud D., 2002, *A&A*, 396, 551
 Maceroni C., Montalbán J., Gandolfi D., Pavlovski K., Rainer M., 2013, *A&A*, 552, A60
 Majewski S. R. et al., 2017, *AJ*, 154, 94
 Matijević G., Prša A., Orosz J. A., Welsh W. F., Bloemen S., Barclay T., 2012, *AJ*, 143, 123
 Matson R. A., Gies D. R., Guo Z., Williams S. J., 2017, *AJ*, 154, 216
 Munari U., Zwitter T., 1997, *A&A*, 318, 269
 Niemczura E. et al., 2015, *MNRAS*, 450, 2764
 Paxton B., Bildsten L., Dotter A., Herwig F., Lesaffre P., Timmes F., 2011, *ApJS*, 192, 3
 Pigulski A., Pojmański G., Pilecki B., Szczygieł D. M., 2009, *Acta Astron.*, 59, 33
 Popper D. M., 1980, *ARA&A*, 18, 115
 Popper D. M., Etzel P. B., 1981, *AJ*, 86, 102
 Popper D. M., Lacy C. H. S., Frueh M. L., Turner A. E., 1986, *AJ*, 91, 383
 Prša A. et al., 2011, *AJ*, 141, 83
 Prusti T. et al. (Gaia Collaboration), 2016, *A&A*, 595, A1
 Randich S., Gilmore G., Gaia-ESO Consortium, 2013, *Msngr.*, 154, 47
 Rawls M. L. et al., 2016, *ApJ*, 818, 108
 Slawson R. W. et al., 2011, *AJ*, 142, 160
 Southworth J., 2015, in Rucinski S. M., Torres G., Zejda M., eds, ASP Conf. Proc. Vol. 486, Living Together: Planets, Host Stars and Binaries. Astron. Soc. Pac., San Francisco, p. 164.
 Southworth J., Maxted P. F. L., Smalley B., 2004a, *MNRAS*, 351, 1277
 Southworth J., Zucker S., Maxted P. F. L., Smalley B., 2004b, *MNRAS*, 355, 986
 Southworth J., Pavlovski K., Tamajo E., Smalley B., West R. G., Anderson D. R., 2011, *MNRAS*, 414, 3740
 Torres G., Andersen J., Giménez A., 2010, *A&AR*, 18, 67
 Wenger M. et al., 2000, *A&AS*, 143, 9
 Worley G., Lee H.-C., 2011, *ApJS*, 193, 1
 Zong W. et al., 2018, *ApJS*, 238, 30
 Zucker S., Mazeh T., 1994, *ApJ*, 420, 806

SUPPORTING INFORMATION

Supplementary data are available at *MNRAS* online.

Table B1. All RVs of SB2 pairs used in this work.

Please note: Oxford University Press is not responsible for the content or functionality of any supporting materials supplied by the authors. Any queries (other than missing material) should be directed to the corresponding author for the article.

APPENDIX A: NEW OBSERVATIONS OF KIC 4758368

Apart from the sample of double- and triple-lined spectroscopic systems, we re-observed KIC 4758368 (KOI 6448), which only shows one set of prominent lines, and was previously described in Paper I. This target is a hierarchical triple, with a short-period ($P \simeq 3.75$ d) eclipsing binary, orbited by a third star on an eccentric, long-period orbit. The third star, which is a red giant, is the dominant source, and we see its lines in spectra. In Paper I, we used our 13 HIDES measurements and six APOGEE data points for the third star, and a set of RVs of the centre of mass of the inner DEB, obtained from its eclipse timing variations (post-ETV RVs). In that work, our data coverage was too short to securely establish the outer period, so we observed this target in 2017 May and July, recording two more spectra. The previous solution predicted a small but measurable rise of the RVs, which would help to constrain the period. Instead, we continued to observe a downward trend, which clearly means the outer period is much longer than what we have obtained previously. The new measurements are listed in Table A1.

As in Paper I, we treated the system as a double-lined binary, with post-ETV RV measurements for one component (designated A), and we directly measured RVs for the other (designated B). We followed the same fitting procedure with V2FIT as previously. Table A2 and Fig. A1 show a comparison of old and new solutions. The most obvious difference is the much longer orbital period, and other parameters dependent on it: $a_{AB} \sin(i)$ and $M_{A,B} \sin^3(i)$. Large relative uncertainty in P also leads to large uncertainties in other parameters.

As in Paper I, we assumed the mass of B to be $1.43 M_{\odot}$ (taken from the *Kepler* Input Catalog) and JKTEBOP results of LC fit (details in Paper I), and we estimated other values, such as the inclination of the outer orbit i_{AB} , its absolute (a_{AB}) and angular (\hat{a}_{AB}) major semi-axes, the total mass of the inner pair M_A and the absolute radii of the inner pair components $R_{Aa,Ab}$. We conclude that the inner pair is likely composed of two subgiant stars, slightly more massive than the Sun, although the uncertainties are very large. Interestingly, the orbital motion of B around a common centre of mass is strong enough to be detectable astrometrically with AO facilities.

There are other estimates of M_B in the literature, reaching up to $2.09 M_{\odot}$. For such a scenario, the inner pair's total mass would be $\sim 4.0 M_{\odot}$, and its components' radii would be $3.0\text{--}3.7 R_{\odot}$, making them comparable in flux or even brighter than the apparently dominant star B. We thus find it unlikely. Other M_B estimates are below solar mass ($0.7\text{--}0.85 M_{\odot}$), but then the system would have to be significantly older than 10 Gyr for B to be a giant.

Table A1. New HIDES RV measurements of KIC 4758368.

BJD 245 0000	v (km s $^{-1}$)	ϵ (km s $^{-1}$)	t_{exp} (s)	S/N
7892.148808	-31.176	0.040	1200	37
7948.177541	-31.394	0.051	900	20

Table A2. New and previous orbital solutions and parameters of KIC 4758368.

Parameter	Paper I	This work
<i>Outer orbit</i>		
P_{AB} (d)	2553(80)	5030(1160)
T_0 (BJD 245 0000)	5581(9)	5570(7)
K_A (km s $^{-1}$)	8.81(41)	8.72(37)
K_B (km s $^{-1}$)	12.9(1.4)	16.8(2.8)
e_{AB}	0.672(37)	0.80(6)
ω_A (°)	142(2)	134(6)
γ (km s $^{-1}$)	-24.0(1.2)	-29.4(1.9)
$M_A \sin^3(i)$ (M_{\odot})	0.65(18)	1.2(7)
$M_B \sin^3(i)$ (M_{\odot})	0.45(9)	0.63(32)
$a_{AB} \sin(i)$ (au)	3.77(32)	9.3(2.1)
N_A	106	106
N_B	19	21
rms_A (km s $^{-1}$)	6.9	6.9
rms_B (m s $^{-1}$)	57	63
<i>JKTEBOP solution</i>		
P_A (d) ^a	3.74993552(43)	
$r_{Aa} + r_{Ab}$	0.4252(64)	
r_{Ab}/r_{Aa}	1.22(21)	
l_B/l_{tot}	0.725	
<i>Absolute values</i>		
d_{GDR2} (pc)		1910(80)
M_B (M_{\odot})		1.43 ^b
i_{AB} (°)	43(5)	50(16)
M_A (M_{\odot})	2.1(6)	2.7(1.6)
a_{AB} (au)	5.54(72)	12(4)
\hat{a}_{AB} (mas)	2.9(4)	6.4(2.0)
a_A (R_{\odot})	13(1)	14(3)
R_{Aa} (R_{\odot})	2.48(35)	2.7(7)
R_{Ab} (R_{\odot})	3.04(27)	3.3(8)

^aOrbital period of the eclipsing inner pair.

^bFrom the KIC values of $\log(g)$ and R given without errors.

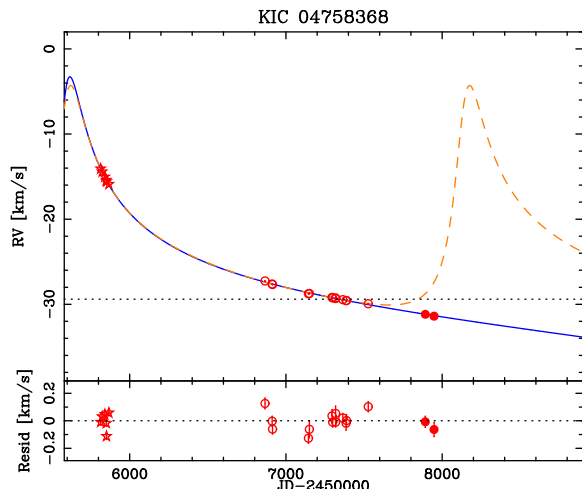


Figure A1. Directly measured RVs of KIC 4758368 B (red symbols), with two orbital solutions: from Paper I (orange dashed line) and this work (blue solid). The APOGEE, old HIDES and new HIDES data are marked with open stars, open circles and filled circles, respectively. The post-ETV velocities of the inner pair A were also used in the fit, but we omit them in the figure for clarity.

APPENDIX B: NEW RV MEASUREMENTS OF SB2 PAIRS

In Table B1, we present individual RV measurements used in this work that were not previously published. TRES and APOGEE data

are properly distinguished. For both components of a given SB2, we show the measured RV values $v_{1,2}$, their errors $\varepsilon_{1,2}$ (both in km s^{-1}), as well as exposure times in seconds and S/N at $\lambda \sim 5500 \text{ \AA}$ for optical spectra, and $\lambda \sim 12000 \text{ \AA}$ for the infrared.

Table B1. All RVs of SB2 pairs used in this work. Complete Table is available in the on-line version of the manuscript.

BJD 245 0000	v_1 (km s^{-1})	ε_1 (km s^{-1})	v_2 (km s^{-1})	ε_2 (km s^{-1})	KIC	t_{exp} (s)	S/N	Note ^a
7673.020510	100.172	0.131	-46.325	0.219	3439031	1500	24	
7812.327593	-50.460	0.137	104.593	0.098	3439031	1500	29	
7846.336225	60.889	0.199	-6.204	0.210	3439031	1500	25	
⋮								
5823.726555	-122.76	6.00	54.11	3.96	4851217	3386	119	A
5849.578427	48.68	5.13	-81.25	5.63	4851217	2002	142	A
5851.648819	-79.27	4.62	13.59	6.14	4851217	2002	134	A
⋮								
6867.030540	-46.473	0.092	13.313	0.145	7821010	1800	48	
6869.142604	-38.627	0.361	5.871	0.532	7821010	1500	23	
6914.079695	-51.604	0.102	18.896	0.132	7821010	1500	63	
⋮								

^aSpectra taken with facilities other than OAO-188cm/HIDES are marked ‘A’ for APOGEE and ‘T’ for TRES.

This paper has been typeset from a $\text{\TeX}/\text{\LaTeX}$ file prepared by the author.